

111
1-65

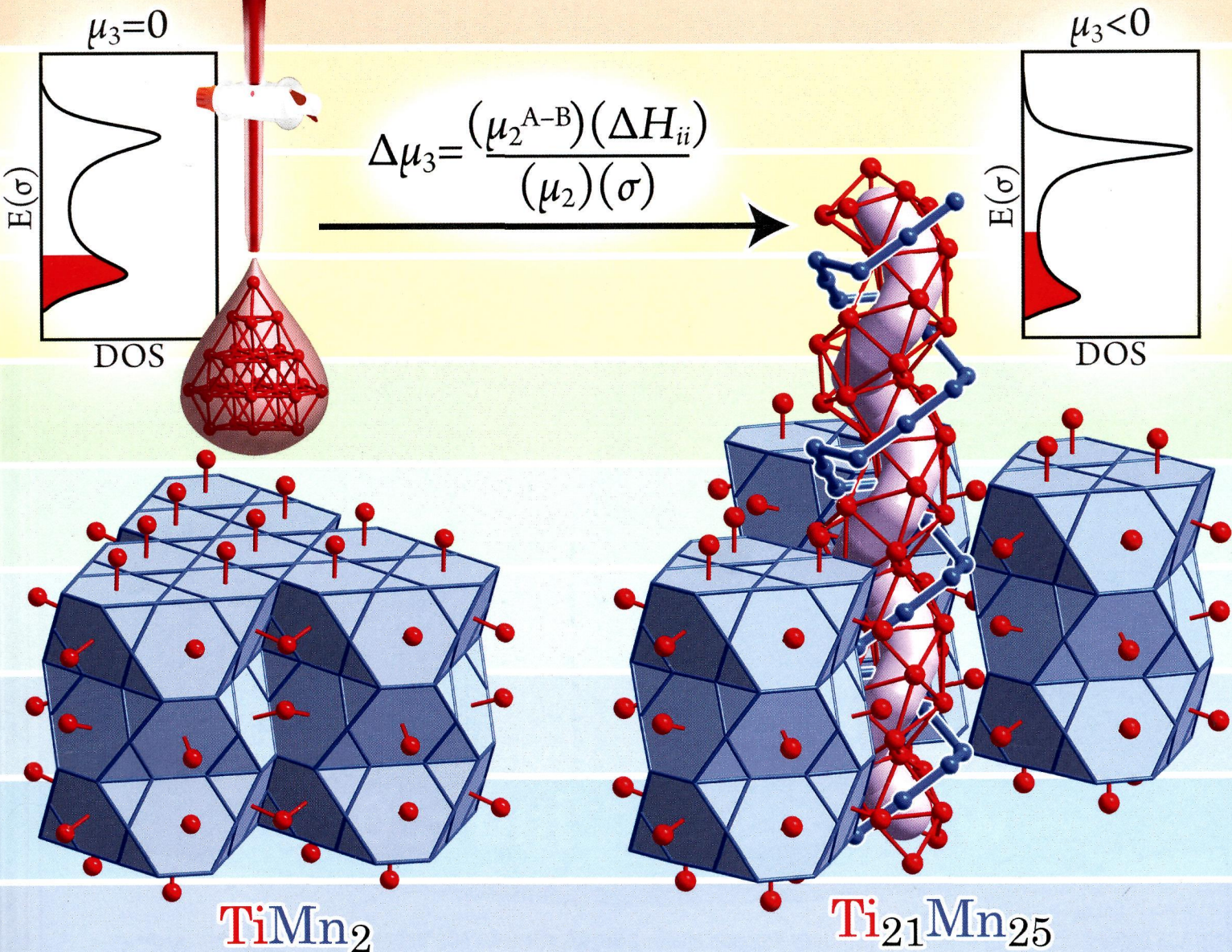
Inorganic Chemistry

including bioinorganic chemistry

August 5, 2013
Volume 52, Number 15
pubs.acs.org/IC

Structural Acid–Base Chemistry in Intermetallics

$$\Delta\mu_3 = \frac{(\mu_2^{A-B})(\Delta H_{ii})}{(\mu_2)(\sigma)}$$



ACS Publications
MOST TRUSTED. MOST CITED. MOST READ.

www.acs.org

ON THE COVER: The Method of Moments and DFT-calibrated Hückel calculations reveal acid–base chemistry in the most unexpected of places: the beautiful and often complex structures of intermetallic phases. Under the newly developed μ_3 -acidity model, TiMn_2 is a well-neutralized adduct of the strong μ_3 -acid Ti and the weaker μ_3 -base Mn. Upon titration in more acidic Ti, the structure responds with the formation of double helices of Ti and Mn to optimize the neutralization of the added Ti, creating the $\text{Ti}_{21}\text{Mn}_{25}$ structure. See T. E. Stacey and D. C. Fredrickson, p 8349.

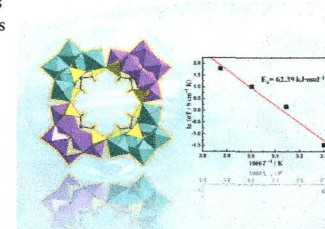
Communications

8285 [dx.doi.org/10.1021/ic400848r](https://doi.org/10.1021/ic400848r)

A Crown-Shaped 24-Molybdate Cluster Constructed by Organotriphosphonate Ligand

Lu Yang, Pengtao Ma, Zhen Zhou, Jingping Wang,* and Jingyang Niu*

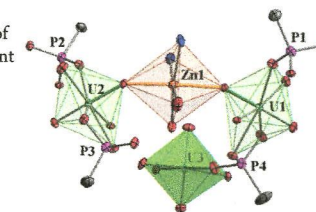
A crown-shaped 24-molybdate cluster constructed by organotriphosphonate was firstly discovered. This compound represents the highest nuclearity of metal atoms in the area of organophosphonate-based polyoxometalates. The ^{31}P NMR spectroscopy, cyclic voltammetry, and proton conductivity are investigated.

8288 [dx.doi.org/10.1021/ic4009834](https://doi.org/10.1021/ic4009834)

Flexible Diphosphonic Acids for the Isolation of Uranyl Hybrids with Heterometallic $\text{U}^{\text{VI}}=\text{O}-\text{Zn}^{\text{II}}$ Cation–Cation Interactions

Tao Tian, Weiting Yang, Hao Wang, Song Dang, and Zhong-Ming Sun*

A family of uranyl diphosphonates have been hydrothermally synthesized using various flexible diphosphonic acids and $\text{Zn}(\text{UO}_2)(\text{OAc})_4 \cdot 7\text{H}_2\text{O}$ in the presence of bipy or phen. Single-crystal X-ray analyses indicate that these compounds represent the first examples of uranyl phosphonates with heterometallic $\text{U}^{\text{VI}}=\text{O}-\text{Zn}^{\text{II}}$ cation–cation interactions.

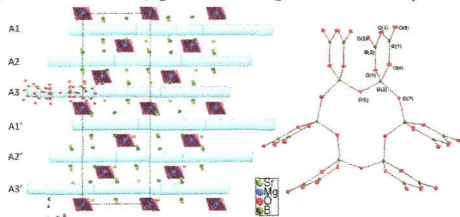


8291  dx.doi.org/10.1021/ic401167z

$\text{Sr}_8\text{MgB}_{18}\text{O}_{36}$: a New Alkaline-Earth Borate with a Novel Zero-Dimensional $(\text{B}_{18}\text{O}_{36})^{18-}$ Anion Ring

Wenjiao Yao, Xingxing Jiang, Hongwei Huang, Tao Xu, Xiaoshan Wang, Zheshuai Lin,* and Chuangtian Chen

Modifying the proportion of different alkaline-earth cations in the $\text{SrO-MgO-B}_2\text{O}_3$ system successfully resulted in a novel borate composed of isolated $(\text{B}_{18}\text{O}_{36})^{18-}$ anionic groups. It is the first time that this building block has been found in a borate. UV-vis-near-IR diffuse-reflectance spectroscopy measurement and first-principles calculations reveal $\text{Sr}_8\text{MgB}_{18}\text{O}_{36}$ to be transparent in the deep-UV region. This work may provide a new path toward the synthesis of deep-UV crystals.

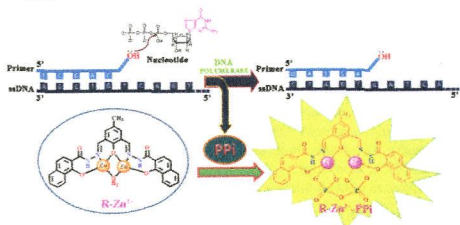


8294  dx.doi.org/10.1021/ic4011696

Naphthalene Carbohydrazone Based Dizinc(II) Chemosensor for a Pyrophosphate Ion and Its DNA Assessment Application in Polymerase Chain Reaction Products

Sellamuthu Anbu,* Subban Kamalraj, Chelliah Jayabaskaran,* and Partha Sarathi Mukherjee*

A Schiff-base-type dizinc(II) complex as a novel, very sensitive, and efficient molecular recognition device not only for the visual and fluorescent sensing of pyrophosphate ions (PPI) in water but also for the discrimination of other anions from PPI with a very low detection limit of 155 ppb has been synthesized and characterized. This has also been used to assess the DNA in polymerase chain reaction products.

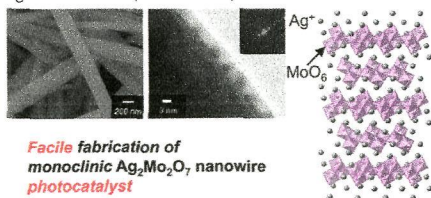


8297  dx.doi.org/10.1021/ic401236b

Monoclinic $\text{Ag}_2\text{Mo}_2\text{O}_7$ Nanowire: A New Ag-Mo-O Nanophotocatalyst Material

Kenji Saito,* Shotaro Kazama, Kazuki Matsubara, Tatsuto Yui, and Masayuki Yagi

A monoclinic $\text{Ag}_2\text{Mo}_2\text{O}_7$ nanowire was developed for the first time by a quite simple strategy using a commercially available MoO_3 particle. The MoO_3 powder was found to induce one-dimensional growth through an oriented aggregation mechanism. Complete structural transformation from bulk to nanowire triggered activity for a photocatalytic O_2 evolution reaction in the presence of AgNO_3 under visible-light irradiation ($\lambda > 400$ nm).

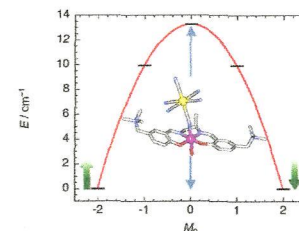


8300  dx.doi.org/10.1021/ic401351w

Slow Relaxation of the Magnetization of an Mn^{III} Single Ion

Ryuta Ishikawa, Ryo Miyamoto, Hiroyuki Nojiri, Brian K. Breedlove, and Masahiro Yamashita*

A new single-ion magnet, Mn^{III} -salen-type complex $[\text{Mn}^{\text{III}}(\text{S-TMAM}(\text{R})\text{-salmen})\text{-(H}_2\text{O)}\text{Co}^{\text{III}}(\text{CN})_6\text{]} \cdot 7\text{H}_2\text{O} \cdot \text{MeCN}$ [1; $\text{S-TMAM}(\text{R})\text{-salmen} = (\text{R})\text{-N,N}'\text{-(1-methylethylene)bis(5-trimethylammoniomethylsalicylideneimine)}$], exhibited slow relaxation of the magnetization.

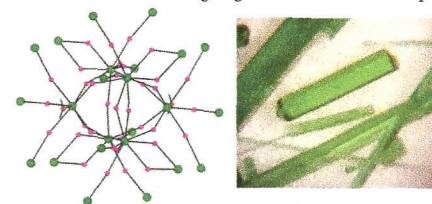


8303  dx.doi.org/10.1021/ic401412t

$\text{U}_3\text{F}_{12}(\text{H}_2\text{O})$, a Noncentrosymmetric Uranium(IV) Fluoride Prepared via a Convenient In Situ Route That Creates U^{4+} under Mild Hydrothermal Conditions

Jeongho Yeon, Mark D. Smith, Athena S. Sefat, T. Thao Tran, P. Shiv Halasyamani, and Hans-Conrad zur Loye*

A new fluoride containing U^{4+} , $\text{U}_3\text{F}_{12}(\text{H}_2\text{O})$, has been synthesized via mild hydrothermal routes. The crystal structure exhibits a complex three-dimensional network composed of hexanuclear building units $[\text{U}_6\text{F}_{33}(\text{H}_2\text{O})_2]^{9-}$. Powder second-harmonic-generation (SHG) measurements revealed that the material shows a weak SHG efficiency. Magnetic property measurements indicated that the U^{4+} cation exhibits a singlet ground state at low temperature.

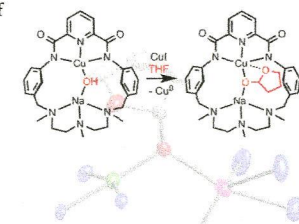


8306  dx.doi.org/10.1021/ic401446s

Isolation of a 2-Hydroxytetrahydrofuran Complex from Copper-Promoted Hydroxylation of THF

Mohammad Reza Halvagar and William B. Tolman*

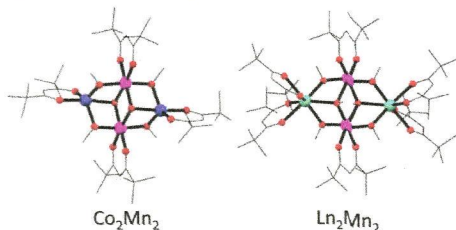
The reaction of a $[\text{Cu}^{\text{II}}(\mu\text{-OH})\text{Na}]^{2+}$ complex with CuI in THF yields a complex of hydroxylated THF, in deprotonated form bridging the Cu^{II} and Na^{I} ions.



New Synthetic Route toward Heterometallic 3d–3d' and 3d–4f Single-Molecule Magnets. The First Co^{II}–Mn^{III} Heterometallic Complex

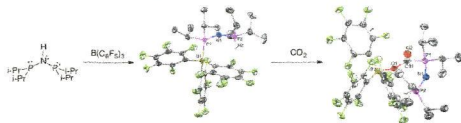
Guilherme P. Guedes, Stéphane Soriano, Luiza A. Mercante, Nivaldo L. Speziali, Miguel A. Novak, Marius Andruh,* and Maria G. F. Vaz*

Four tetranuclear heterometallic complexes with the molecular formulas [Co^{II}Mn^{III}(dpm)₄(MeO)₆] (**1**) and [Ln^{III}₂Mn^{III}₂(dpm)₆(MeO)₆(MeOH)_{*n*}] where Ln = Gd (**2**, *n* = 2), Tb (**3**, *n* = 2), and Dy (**4**, *n* = 0) were obtained by a one-pot reaction. The crystal structure of the four complexes consists of a M₂Mn₂ core, in which metal ions and the bridging methoxy groups describe a defect-diheterocubane architecture. Magnetic measurements revealed that compounds **1**, **3**, and **4** present slow relaxation of the magnetization at low temperatures.

**NH/PH Isomerization and a Lewis Pair for Carbon Dioxide Capture**

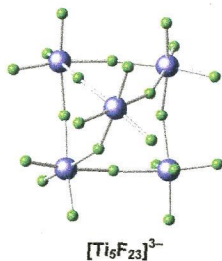
Brian M. Barry, Diane A. Dickie, Luke J. Murphy, Jason A. C. Clyburne,* and Richard A. Kemp*

The ligand (*i*-Pr₂P)₂NH reacts with the strong Lewis acid B(C₆F₅)₃ to form an adduct, resulting in H-isomerization from N to P. This complex reacts easily with CO₂ in a manner reminiscent of frustrated Lewis pairs and attempts to prepare anionic derivatives led to activation of a C–F bond and formation of a novel heterocycle.

**Articles****Crystal Structures and Raman Spectra of Imidazolium Poly[perfluorotitanate(IV)] Salts Containing the [TiF₆]²⁻, [(Ti₂F₉)₂]⁴⁻, and [Ti₂F₁₁]³⁻ and the New [Ti₄F₂₀]⁴⁻ and [Ti₅F₂₃]³⁻ Anions**

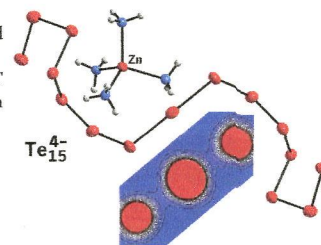
Igor M. Shlyapnikov, Hélène P. A. Mercier, Evgeny A. Goreschnik, Gary J. Schrobilgen,* and Zoran Mazej*

Reactions of imidazole (Im) and TiF₄ in varying molar ratios in a HF solvent have afforded the X-ray structures of five new fluorotitanate salts of the imidazolium cation, ImH⁺: [ImH]₂[TiF₆]·2HF, [ImH]₃[Ti₂F₁₁], [ImH]₄[Ti₄F₂₀], [ImH]₃[Ti₃F₂₃], and [ImH]₂[Ti₂F₉]. The [Ti₄F₂₀]⁴⁻ and [Ti₅F₂₃]³⁻ anions are novel and have structures comprised of four and five TiF₆ octahedra, respectively. The poly[perfluorotitanate(IV)] anions have also been characterized by Raman spectroscopy ([Ti₂F₉]²⁻, [Ti₄F₂₀]⁴⁻, and [Ti₅F₂₃]³⁻) and quantum-chemical calculations ([Ti₄F₂₀]⁴⁻ and [Ti₅F₂₃]³⁻).

**Polytellurides of Mn, Fe, and Zn from Mild Solvothermal Reactions in Liquid Ammonia**

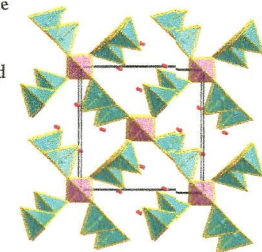
Oleksandr Kysliak, Max Marcus, Thomas Bredow, and Johannes Beck*

Elemental Mn, Fe, and Zn react with Te in liquid ammonia at 50 °C to form metal–amine polytellurides [Mn(NH₃)₆]_{*n*}Te₄ (**1**), [Fe(NH₃)₆]_{*n*}Te₄NH₃ (**2**), and [Zn(NH₃)₄]_{*n*}Te₁₅ (**3**). The structures of the semiconducting compounds contain concatenated polytelluride ions with characteristic linear Te₃ groups. Periodic DFT calculations show that interaction between the Te₄²⁻ units is highly dependent on the Te–Te distances and negligible in **1**, present in **2**, and significant in the symmetrical (Te₁₅)⁴⁻ chain of **3**.

**Syntheses, Structures, and Nonlinear Optical Properties of Quaternary Chalcogenides: Pb₄Ga₄GeQ₁₂ (Q = S, Se)**

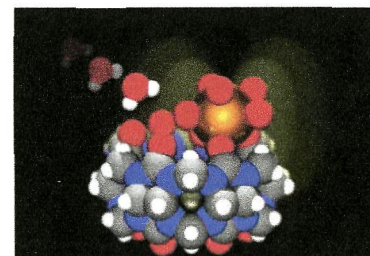
Yu-Kun Chen, Mei-Chun Chen, Liu-Jiang Zhou, Ling Chen, and Li-Ming Wu*

Two noncentrosymmetric compounds Pb₄Ga₄GeQ₁₂ (Q = S, Se) are characterized by the three-dimensional framework constructed by chains of GaQ₄ tetrahedra that are interconnected by separated GeQ₄ tetrahedra at regular intervals. Interestingly, such a [Ga₄GeQ₁₂]⁸⁻ framework is flexible to allow the embedded two types of vacancies occupied by Ag⁺ or Li⁺ without symmetry breaking. Pb₄Ga₄GeSe₁₂ shows strong powder second-harmonic generation, that is 2X commercial AgGaS₂ at 2.05 μm.

**Dy(III) Single-Ion Magnet Showing Extreme Sensitivity to (De)hydration**

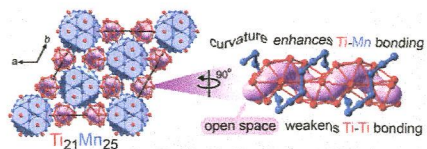
Min Ren, Dawid Pinkowicz,* Minyoung Yoon, Kimoon Kim, Li-Min Zheng, Brian K. Breedlove, and Masahiro Yamashita*


A new mononuclear dysprosium(III)-cucurbit[6]uril complex has been synthesized and characterized structurally and magnetically. It exhibits single-ion magnet (SIM) behavior with two slow magnetic relaxation processes, which are very sensitive to the solvation degree of the sample. Depending on the amount and type of the solvent in the structure, it is possible to switch the slow magnetic relaxation of this compound between the temperature-independent and temperature-dependent regimes.



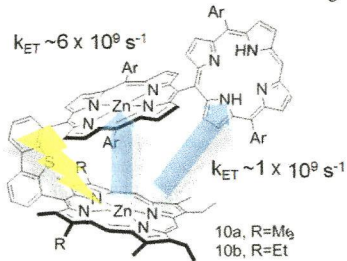
8349  dx.doi.org/10.1021/ic302619h
Structural Acid–Base Chemistry in the Metallic State: How μ_3 -Neutralization Drives Interfaces and Helices in $Ti_{21}Mn_{25}$
 Timothy E. Stacey and Daniel C. Fredrickson*


Intermetallic phases remain a large class of compounds whose vast structural diversity is unaccounted for by chemical theory. A recent resurgence of interest in intermetallics has intensified the need for models connecting their compositions to their structures and stability. We illustrate how the μ_3 -acidity model, an extension of the acid/base concept based on the Method of Moments, offers intuitive explanations for puzzling structural progressions occurring in intermetallics formed between transition metals.



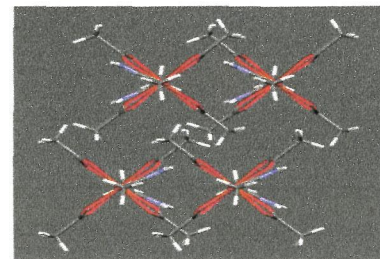
8360  dx.doi.org/10.1021/ic3026655
Design of Triads for Probing the Direct Through Space Energy Transfers in Closely Spaced Assemblies
 Jean-Michel Camus, Shawkat M. Aly, Daniel Fortin, Roger Guilard,* and Pierre D. Harvey*


Trimers with a $D^*A_1-A_2$ structure where the donor **D** (octa- β -alkyl zinc(II)porphyrin) transfers its S_1 energy to two different acceptors, di(4-ethylbenzene) zinc(II)porphyrin (A_1) placed face-to-face with **D**, and the corresponding free base (A_2), which is *meso-meso*-linked with A_1 , were synthesized using a selective stepwise Suzuki cross-coupling reaction. Two paths of S_1 energy transfer for the global process $D^* \rightarrow A_2$: (1) $D^* \rightarrow A_1 \rightarrow A_2$, (2) direct through space $D^* \rightarrow A_2$.



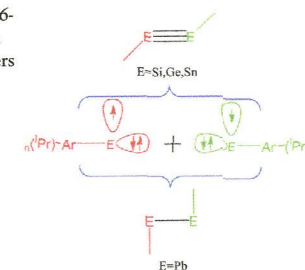
8369  dx.doi.org/10.1021/ic3027804
Unusual Conformation of a Dinuclear Paddle Wheel Copper(II) Complex. Synthesis, Structural Characterization and EPR Studies


Verónica Paredes-García,* Ricardo C. Santana,* Rosa Madrid, Andrés Vega, Evgenia Spodine, and Diego Venegas-Yazigi
 An unusual and unique conformation of a paddle wheel type binuclear copper(II) complex, containing acetate and acetamido ligands, $\{Cu_2(\mu_2-O_2CCH_3)_4\}(OCNH_2CH_3)$ (**1**), was obtained by solvothermal synthesis. $Cu_2(\mu_2-O_2CCH_3)_4(OCNH_2CH_3)$, was structurally and magnetically characterized using EPR spectroscopy. Through the powder and single crystal EPR measurements it was possible to evaluate the magnetic exchange couplings and the fine structure parameters. The intraduclear exchange coupling of -101 cm^{-1} is smaller than the one observed in other Cu^{II} -PW units.

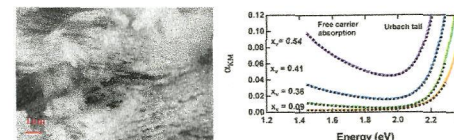


8378  dx.doi.org/10.1021/ic401149h
Role Played by Isopropyl Substituents in Stabilizing the Putative Triple Bond in Ar^*EEAr' [E = Si, Ge, Sn; $Ar' \approx C_6H_3-2,6-(C_6H_3-2,6-Pr_2)_2$ and $Ar^*PbPbAr^*$ [$Ar^* = C_6H_3-2,6-(C_6H_2-2,4,6-Pr_3)_2$]
 Issaka Seidu, Michael Seth, and Tom Ziegler*

NOCV–ETS analysis of the E–E bonding in Ar^*EEAr' [E = Si, Ge, Sn; $Ar' = C_6H_3-2,6-(C_6H_3-2,6-Pr_2)_2$] and $Ar^*PbPbAr^*$ [$Ar^* = C_6H_3-2,6-(C_6H_2-2,4,6-Pr_3)_2$] revealed a triple bond for E = Si, Ge, and Sn and a single bond for E = Pb. The Ar^*EEAr' dimers were found to be stabilized substantially by van der Waals dispersion interactions between isopropyl groups attached to Ar groups on different E centers.



8389  dx.doi.org/10.1021/ic400011n
Synthesis and Characterization of Visible Light Absorbing $(GaN)_{1-x}(ZnO)_x$ Semiconductor Nanorods
 Alexandra A. Reinert, Candace Payne, Limin Wang, James Ciston, Yimei Zhu, and Peter G. Khalifah*
 “Carpet” of $(GaN)_{1-x}(ZnO)_x$ nanorods prepared from $Ga_2O_3(ZnO)_{16}$ precursors, samples which have direct band gaps as low as 2.5 eV depending on the Zn content (maximum of ~55%). The midgap absorption of these samples can be quantitatively fit (black dashes) to a combination of an Urbach tail (exponential decay) and free carrier absorption which increases as λ^3 due to ionized impurity scattering.

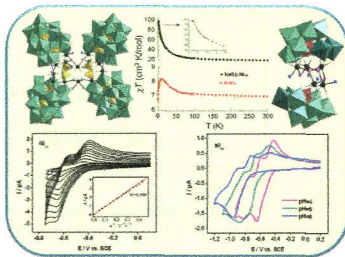


Synthesis, Magnetism, and Electrochemistry of the Ni₁₄- and Ni₅-Containing Heteropolytungstates

[Ni₁₄(OH)₆(H₂O)₁₀(HPO₄)₄(P₂W₁₅O₅₆)₄]³⁴⁻ and [Ni₅(OH)₄(H₂O)₄(β-GeW₉O₃₄)(β-GeW₆O₃₀(OH))]¹³⁻

Masooma Ibrahim, Yixian-Xiang, Bassem S. Bassil, Yanhua Lan, Annie K. Powell,* Pedro de Oliveira, Bineta Keita, and Ulrich Kortz*

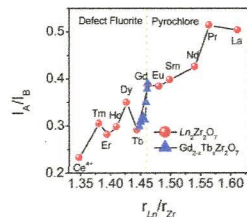
Reaction of Ni²⁺ ions with trilacunary Wells–Dawson and dilacunary Keggin precursors resulted in the tetradeca- and pentanickel(II)-containing heteropolyanions [Ni₁₄(OH)₆(H₂O)₁₀(HPO₄)₄(P₂W₁₅O₅₆)₄]³⁴⁻ (Ni₁₄) and [Ni₅(OH)₄(H₂O)₄(β-GeW₉O₃₄)(β-GeW₆O₃₀(OH))]¹³⁻ (Ni₅), respectively. Both polyanions were prepared via conventional synthetic procedures and characterized by various solution and solid state analytical techniques.



Anion Disorder in Lanthanoid Zirconates Gd_{2-x}Tb_xZr₂O₇

Emily Reynolds, Peter E. R. Blanchard, Brendan J. Kennedy,* Chris D. Ling, Samuel Liu, Max Avdeev, Zhaoming Zhang, Gabriel J. Cuello, Anton Tadić, and Ling-Yun Jang

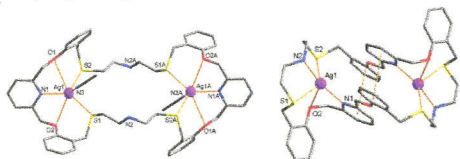
Changes in the local and average structure due to the fluorite–pyrochlore transition in Gd_{2-x}Tb_xZr₂O₇ are monitored using neutron and X-ray diffraction and X-ray spectroscopy.



Endo- and Exocyclic Supramolecular Complexes of Mixed-Donor Macrocycles via [1:1] and [2:2] Cyclizations

Seul-Gi Lee, Ki-Min Park, Yoichi Habata, and Shim Sung Lee*

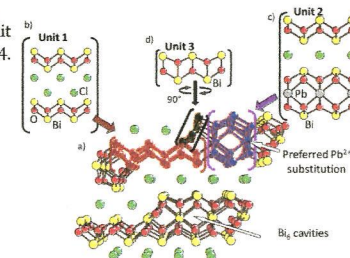
In complexation of a 40-membered N₄O₄S₄ macrocycle L² with AgNO₃, two endocyclic dinuclear complexes [Ag₂(L²)(CH₃CN)₂](NO₃)₂ and [Ag₂(L²)](NO₃)₂ with different coordination environments were isolated as kinetic and thermodynamic controlled products, respectively.



New [PbBi₂O₄][Bi₂O₂]Cl₂ and [Pb_nBi_{10-n}O₁₃][Bi₂O₂]_nCl_{4+n} Series by Association of Sizable Subunits: Relationship with Arppe's Compound Bi₂₄O₃₁Cl₁₀ and Luminescence Properties

A. Aliev, J. Olchowka, M. Colmont, E. Capoen, C. Wickleder, and O. Mentré*

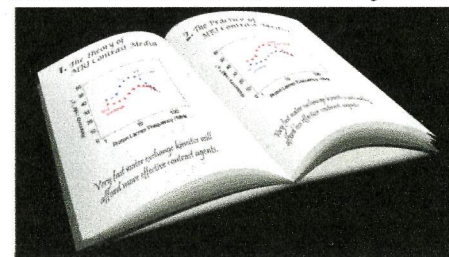
The new series [Pb_nBi_{10-n}O₁₃][Bi₂O₂]_nCl_{4+n} is strongly related to Bi₂₄O₃₁Cl₁₀ well-known as the Arppe's compound in which the fluorite-like [Bi₂O₂]_n subunit was increased from n = 1 (mixed Bi/Pb Arppe's compound) to n = 2, 3, and 4. The Bi/Pb and oxygen ordering is discussed as well as ionic transport and luminescent properties.



Coupling Fast Water Exchange to Slow Molecular Tumbling in Gd³⁺ Chelates: Why Faster Is Not Always Better

Stefano Avedano, Mauro Botta,* Julian S. Haigh, Dario L. Longo, and Mark Woods*

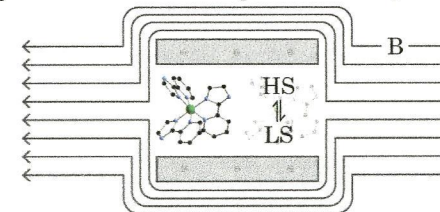
Theory often leads to an expectation that very fast water exchange is required to afford the highest relaxivity Gd³⁺ chelate. In practice, of two isomeric Gd³⁺ chelates, the one with the slowest water exchange affords the highest relaxivity.



Hybrid Magnetic Superconductors Formed by TaS₂ Layers and Spin Crossover Complexes

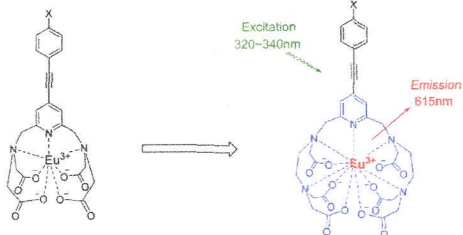
Eugenio Coronado,* Mónica Giménez-Marqués, Carlos Martí-Gastaldo, Guillermo Mínguez Espallargas, Efrén Navarro-Moratalla, and João C. Waerenborgh

The solid-state/molecule-based hybrid approach has been herein employed for the chemical design and synthesis of a layered material that includes superconducting (SC) TaS₂ layers and Fe²⁺ complexes with spin crossover (SCO) properties. The delamination/flocculation synthetic approach permits us here to isolate a crystallographically pure hybrid material in the form of highly oriented free-standing flakes that mimic the anisotropic behavior of the parent TaS₂ crystals.



Stable and Highly Fluorescent Europium(III) Chelates for Time-Resolved ImmunoassaysQi Wang,* Katia Nchimi Nono, Markku Syrj n p  , Lo c J. Charbonni re, Jari Hovinen, and Harri H rm *

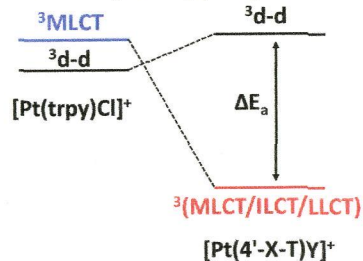
Easy-to-make chelating structures that form europium(III) complexes with excellent aqueous solubility and stability have been prepared. The fluorescence quantum yield is exceptionally high and lifetime long, making these chelates potent labeling reagents that increase the sensitivity and detection limit of present immunoassays and allow the development of new ones.

**A Diruthenium Complex of a "Nindigo" Ligand**Prasenjit Mondal, Fabian Ehret, Martina Bubrin, Amit Das, Shaikh M. Mobin, Wolfgang Kaim,* and Goutam Kumar Lahiri*

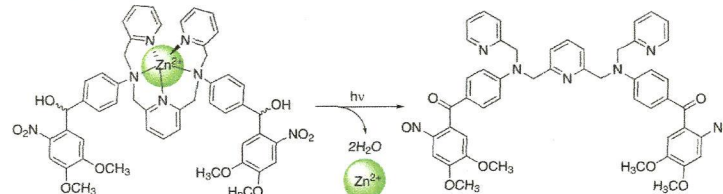
The compound $\{(\mu\text{-Nindigo})[\text{Ru}(\text{acac})_2]_2\} = \mathbf{1}$, $\text{H}_2(\text{Nindigo}) = \text{indigo-}N,N'$ -diphenylimine and $\text{acac}^- = 2,4\text{-pentanedionate}$, has been structurally characterized in the *rac* form, which exhibits two edge-sharing six-membered chelate rings involving ruthenium, and the former β -diketiminato functions with a twist angle of 33.9° around the central C–C bond. The metric parameters suggest a neutral π acceptor bridge containing coupled *s-trans* configured α -diimines, which are coordinated by two ruthenium(II) centers.

 **π Donation and Its Effects on the Excited-State Lifetimes of Luminescent Platinum(II) Terpyridine Complexes in Solution**Lauren M. Hight, Meaghan C. McGuire, Yu Zhang, Matthew A. Bork, Phillip E. Fanwick, Adam Wasserman, and David R. McMillin*

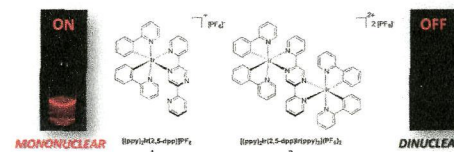
Tuning the coligand and the 4'-substituent can enhance emission from platinum(II) terpyridines by state mixing and/or bolstering LF strength. Changing the coligand and/or adding a π -electron-donating substituent in the 4'-position of the terpyridine ligand can enhance the emission from a platinum(II) complex.

**Increasing the Dynamic Range of Metal Ion Affinity Changes in Zn^{2+} Photocages Using Multiple Nitrobenzyl Groups**Celina Gwizdala, Prem N. Basa, John C. MacDonald, and Shawn C. Burdette*

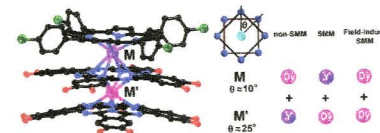
DiCast-1, -2, and -3 are metal ion chelators that contain two aniline ligands each connected to a nitrobenzhydryl photocaging group. Photolysis converts the benzhydryl into an electron withdrawing ketone, which decreases the electron density on the nitrogen atom since it is located *para* to the aniline group. The modification of the chelator decreases the binding affinity for the metal ion guest. Compared to earlier photocages with a single nitrobenzhydryl group, the change in metal binding affinity is an order of magnitude larger.

**Mono- and Dinuclear Cationic Iridium(III) Complexes Bearing a 2,5-Dipyridylpyrazine (2,5-dpp) Ligand**Loic Donato, Catherine E. McCusker, Felix N. Castellano,* and Eli Zysman-Colman*

Mononuclear (**1**) and dinuclear (**2**) cationic iridium complexes incorporating a bridging 2,5-dipyridylpyrazine ligand have been synthesized and their optoelectronic properties are characterized. Whereas **1** emits in the deep red, **2** is photophysically inactive at 298 K though both luminesce at 77 K in a rigid matrix. The crystal structures for both complexes are also reported.

**Sandwich-Type Mixed Tetrapyrrole Rare-Earth Triple-Decker Compounds. Effect of the Coordination Geometry on the Single-Molecule-Magnet Nature**Jinglan Kan, Hailong Wang, Wei Sun, Jun Tao, and Jianzhuang Jiang*

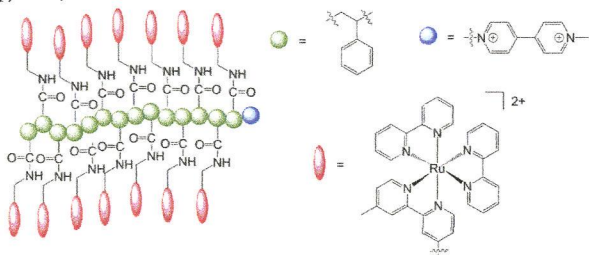
Systematic and comparative studies revealed magnetic-field-induced single-molecule magnet (SMM), SMM, and non-SMM nature for the mixed tetrapyrrole complexes of Dy–Dy, Y–Dy, and Dy–Y, respectively, indicating the dominant effect of the coordination geometry of the spin carrier, actually the twist angle between the two tetrapyrrole rings, instead of the f – f interaction on the SMM nature.



Atom Transfer Radical Polymerization Preparation and Photophysical Properties of Polypyridylruthenium Derivatized Polystyrenes

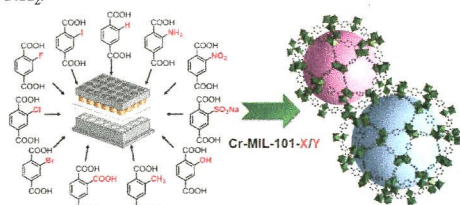
Zhen Fang, Akitaka Ito, Shahar Keinan, Zuofeng Chen, Zoe Watson, Jason Rochette, Yosuke Kanai, Darlene Taylor, Kirk S. Schanze, and Thomas J. Meyer*

A metallopolymer structure featuring a short carbonyl-amino-methylene linker has been prepared by atom transfer radical polymerization (ATRP). The polymer was derived from ATRP of the N-hydroxysuccinimide (NHS) derivative of *p*-vinylbenzoic acid, followed by an amide coupling reaction of the NHS-polystyrene with Ru(II) complexes derivatized with aminomethyl groups (i.e. $[\text{Ru}(\text{bpy})_2(\text{CH}_3\text{-bpy-CH}_2\text{NH}_2)]^{2+}$ where bpy is 2,2'-bipyridine, and $\text{CH}_3\text{-bpy-CH}_2\text{NH}_2$ is 4-methyl-4'-aminomethyl-2,2'-bipyridine).

**Single- and Mixed-Linker Cr-MIL-101 Derivatives: A High-Throughput Investigation**

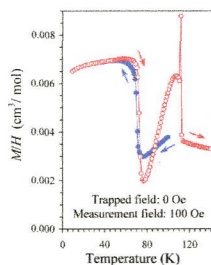
Martin Lammert, Stephan Bernrt, Frederik Vermoortele, Dirk E. De Vos, and Norbert Stock*

New single- and mixed-linker Cr-MIL-101 derivatives bearing different functional groups, -F, -Cl, -Br, -NH₂, -NO₂, -H, -SO₃H, -CH₃, and -COOH, have been synthesized. High-throughput methods were employed to investigate the influence of the metal source (CrO₃, CrCl₃, and Cr(NO₃)₃·9H₂O), the linker functionalization, and the use of mixtures of linkers on product formation. Postsynthetic modification was successfully carried out to selectively reduce the mixed-linker compound Cr-MIL-101-Br-NO₂ to Cr-MIL-101-Br-NH₂.

**Fresh Look at the Mystery of Magnetization Reversal in YVO₃**

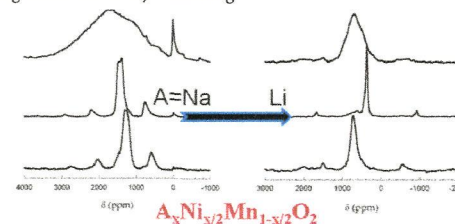
Alexei A. Belik*

Magnetic properties of different polycrystalline YVO₃ samples were studied. A remarkable exchange bias effect was observed in all samples. Tunable exchange bias was suggested to be the origin of magnetization reversal in YVO₃. The results provide significant contribution to understanding the mystery of the magnetization reversal effects in YVO₃ and allow looking at the problem from a different viewpoint.

**Study of the Transition Metal Ordering in Layered Na_xNi_{x/2}Mn_{1-x/2}O₂ (2/3 ≤ x ≤ 1) and Consequences of Na/Li Exchange**

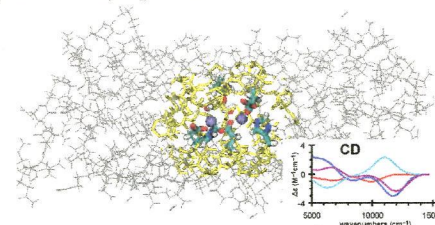
Jordi Cabana,* Natasha A. Chernova, Jie Xiao, Megan Roppolo, Kellie A. Aldi, M. Stanley Whittingham, and Clare P. Grey*

A study of the long and short-range structure of layered oxides within the Na_xNi_{x/2}Mn_{1-x/2}O₂ (2/3 ≤ x ≤ 1) system was undertaken. A transition from P to O stacking and disordering of ions in the transition metal layer was observed at x > 0.8. Na/Li exchange largely preserved the transition metal ordering, but led to Li/Ni crystallographic exchange in O3 phases, as well as the formation of stacking faults due to layer shearing.

**QM/MM Structural and Spectroscopic Analysis of the Di-iron(II) and Di-iron(III) Ferroxidase Site in M Ferritin**

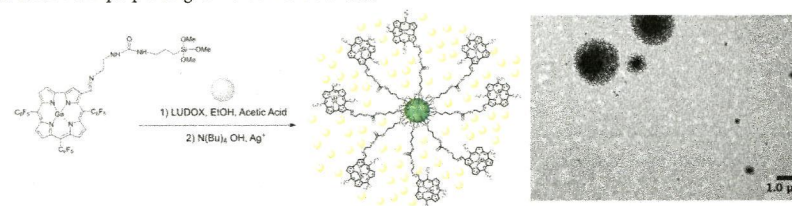
Travis V. Harris and Keiji Morokuma*

The ONIOM method is used to identify the iron(II)- and iron(III)-bound structures of the frog M ferritin ferroxidase site. Calculated exchange couplings (*J*), Mössbauer parameters, and time-dependent density functional theoretical (TD-DFT) circular dichroism spectra are compared with the available experimental data. For the di-iron(II) site, we find that Asp140 is coordinated, whereas Gln137 is not. For the di-iron(III) products, we find that a μ -oxo-bridged and two doubly bridged (μ -hydroxo and μ -oxo/hydroxo) species are likely coproduced.

**Corrole and Corrole Functionalized Silica Nanoparticles as New Metal Ion Chemosensors: A Case of Silver Satellite Nanoparticles Formation**

Carla I. M. Santos, Elisabete Oliveira,* Javier Fernández-Lodeiro, Joana F. B. Barata, Sérgio M. Santos, M. Amparo F. Faustino, José A. S. Cavaleiro, M. Graça P. M. S. Neves,* and Carlos Lodeiro*

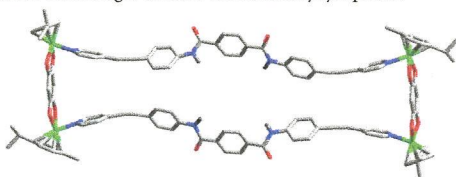
Corrole 1 was studied in the presence Ag⁺, Na⁺, Ca²⁺, Zn²⁺, Cd²⁺, Cu²⁺, Pb²⁺, Hg²⁺, Zn²⁺, Ni²⁺, Cr³⁺, Ga³⁺, Fe³⁺, and Al³⁺ metal ions in toluene and acetonitrile. In toluene, the species corrole 1⁻ shows to be a naked eye sensor in the presence of Hg²⁺; a change of color from dark green to green was observed. Also, corrole 1 reveals to be selective for Hg²⁺ in acetonitrile, where a change of color from purple to green-blue was observed.



8573  dx.doi.org/10.1021/ic401685s
Synthesis and Characterization of Self-Assembled Nanoscopic Metallarectangles Capable of Binding Fullerenes with Size-Selective Responses

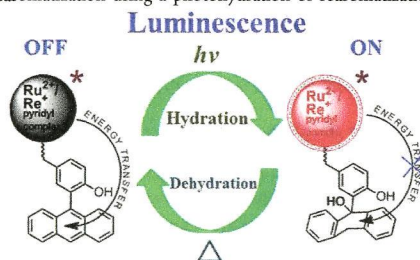
Anurag Mishra, Hyunji Jung, Min Hyung Lee, Myoung Soo Lah, and Ki-Whan Chi*

Two new metallarectangles, 4 and 5, were obtained from the self-assembly of areneruthenium-based molecular clips 2 and 3 with a new dipyriddy donor ligand 1 containing a diamide core and ethynyl spacers.



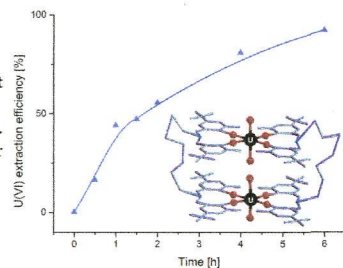
8579  dx.doi.org/10.1021/ic400676j
ON-OFF Luminescence Signaling of Hybrid Organic–Inorganic Switches
 Palani Natarajan* and Michael Schmittel*


Two hybrid organic–inorganic switches were prepared by linking prototypical ruthenium or rhenium luminophores to the 2-(anthracen-9-yl)-4-methylphenol unit as a switchable photoactive moiety. Emission of the inorganic luminophore was reversibly switched ON and OFF multiple times by adjusting the energetic level of the $^3\pi-\pi^*$ state of the appended anthracene unit through either dearomatization using a photohydration or rearomatization applying a thermal dehydration.



8591  dx.doi.org/10.1021/ic400663y
Uranyl Complexes of Alkyl-Bridged Ditopic Diaminotetraphenol Ligands and Their Use as Uranyl Ion Extractors
 Antti Riisö, Ari Väisänen, and Reijo Sillanpää*

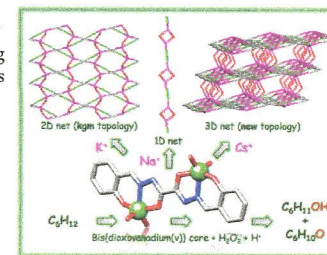
The coordination chemistry of uranyl ions was studied using ditopic diaminotetraphenols (H_4L1-H_4L4), which form 2:1 (U-to-L ratio) complexes. The 2:1 complexes are neutral $[(UO_2)_2(H_2Lm)(NO_3)_2(solvent)_2]$ or anionic $[(UO_2)_2(H_2Lm)(NO_3)_2(anion)_2]^{2-}$. In the 2:1 complexes, the uranyl ions are at both ends of the ligand. H_4L2 and H_4L3 form also cyclic (1:1) dinuclear molecules. The best uranyl ion extractor from water to dichloromethane is H_4L3 . In the presence of Cu^{II} , Ni^{II} , Co^{II} , and Zn^{II} ions, the best extraction selectivity for uranyl ions was found with H_4L1 .



8601  dx.doi.org/10.1021/ic400743h
Alkali Metal Directed Assembly of Heterometallic V^V/M ($M = Na, K, Cs$) Coordination Polymers: Structures, Topological Analysis, and Oxidation Catalytic Properties

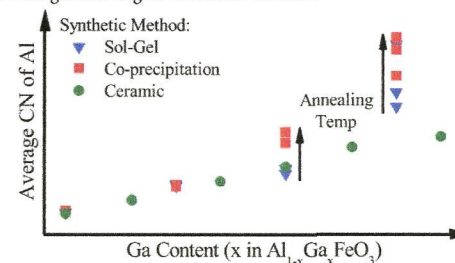
Samik Gupta, Marina V. Kirillova, M. Fátima C. Guedes da Silva,* Armando J. L. Pombeiro,* and Alexander M. Kirillov*

New heterometallic V^V/M ($M = Na, K, Cs$) coordination polymers bearing divanadium(V) cores and alkali metal aqua moieties were synthesized and fully characterized, revealing distinct 1D, 2D, and 3D coordination networks, including a topologically unique example. These compounds also act as efficient precatalysts for the mild oxidation of cyclohexane.



8612  dx.doi.org/10.1021/ic4007636
The Effect of Synthetic Method and Annealing Temperature on Metal Site Preference in $Al_{1-x}Ga_xFeO_3$
 James D. S. Walker and Andrew P. Grosvenor*

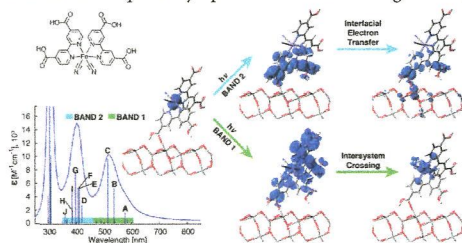
The ferrimagnetic and piezoelectric $Al_{1-x}Ga_xFeO_3$ ($0 \leq x \leq 1$) system owes its properties to cation antisite disorder. These materials were synthesized by the sol–gel and coprecipitation methods, and studied using X-ray absorption spectroscopy to monitor changes in the average coordination number of the constituent metals. Changes in composition had a greater effect on the metal coordination number than synthetic method or annealing temperature. Further, materials synthesized by the coprecipitation method showed the greatest degree of antisite disorder.



Elucidating Band-Selective Sensitization in Iron(II) Polypyridine-TiO₂ Assemblies

David N. Bowman, James H. Blew, Takashi Tsuchiya, and Elena Jakubikova*

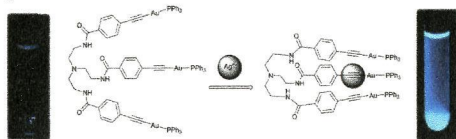
A computational study employing density functional and time-dependent density functional approaches as well as quantum dynamics simulations is used to model Fe(II)-polypyridine complexes adsorbed to a TiO₂ surface via carboxylic acid linkers or cyanide ligands. All complexes investigated display two absorption bands in the visible region. The results elucidate band-selective sensitization in [Fe(II)(2,2'-bipyridine-4,4'-dicarboxylic acid)₂(CN)₂]-TiO₂ assemblies, in which interfacial electron transfer into the TiO₂ conduction band occurs primarily upon excitation of the higher energy absorption band.



Highly Ag⁺ Selective Tripodal Gold(I) Acetylide-based "Off-On" Luminescence Chemosensors based on ³(ππ*) Emission Switching

Yu-Peng Zhou, En-Bao Liu, Jin Wang, and Hsiu-Yi Chao*

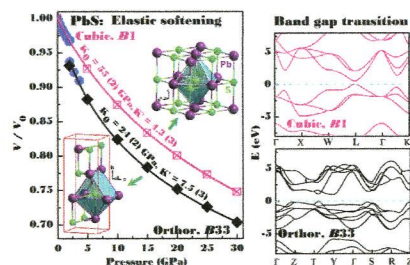
Gold(I) acetylide chemosensor **1c** possesses acetylide groups that act as selective and sensitive Ag⁺ receptor pockets. Probe **1c** exhibits high analyte selectivity against other interferents and acts as a novel "off-on" (³(ππ*) luminescent switch toward Ag⁺.



Phase-Transition Induced Elastic Softening and Band Gap Transition in Semiconducting PbS at High Pressure

Shanmin Wang, Jianzhong Zhang, Yi Zhang, Andrew Alvarado, Jeevake Attapattu, Duanwei He,* Liping Wang, Changfeng Chen, and Yusheng Zhao*

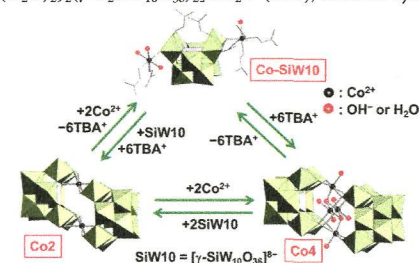
Observation of phase-transition induced elastic softening in PbS correlated with direct-to-indirect band gap transition at high pressure.



Synthesis, Structure Characterization, and Reversible Transformation of a Cobalt Salt of a Dilacunary γ -Keggin Silicotungstate and Sandwich-Type Di- and Tetracobalt-Containing Silicotungstate Dimers

Yuji Kikukawa, Kosuke Suzuki, Kazuya Yamaguchi, and Noritaka Mizuno*

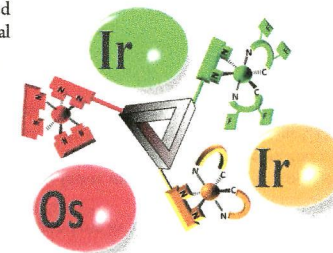
A cobalt salt of a γ -Keggin dilacunary silicotungstate, {CoL₅}₂[γ -SiW₁₀O₃₄L₂] (Co-SiW10; L = DMF or H₂O), could be synthesized by the cation-exchange reaction of TBA₄[γ -H₄SiW₁₀O₃₆] (TBA = tetra-*n*-butylammonium) with 2 equiv of Co(NO₃)₂ with respect to TBA₄[γ -H₄SiW₁₀O₃₆]. By the reaction of Co-SiW10 with 1 equiv of TBA₆[γ -H₂SiW₁₀O₃₆], a silicotungstate dimer pillared by two cobalt cations, TBA₆[Co₂(γ -H₃SiW₁₀O₃₆)₂]-3H₂O (Co₂), could be synthesized. By the reaction of Co-SiW10 with 3 equiv of TBAOH in acetone, a tetracobalt-containing sandwich-type silicotungstate, TBA₆[{Co(H₂O)}₂(μ_3 -OH)₂{Co(H₂O)₂}(γ -H₂SiW₁₀O₃₆)₂]-5H₂O (Co₄), could be synthesized.



Multichromophoric Arrays Arranged around a Triptycene Scaffold: Synthesis and Photophysics

Thomas Bura, Maria Pia Gullo, Barbara Ventura, Andrea Barbieri,* and Raymond Ziessel*

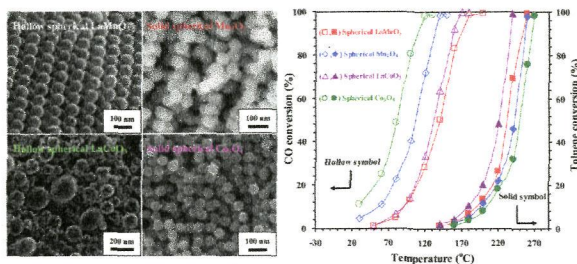
Star-shaped 3D arrays based on a rigid photoactive triptycene scaffold decorated with Ir(III) and Os(II) satellite complexes have been designed to show an ideal cascade for fast and efficient energy collection and transfer to the lowest-lying excited state.




8665  dx.doi.org/10.1021/ic400832h

Controlled Generation of Uniform Spherical LaMnO₃, LaCoO₃, Mn₂O₃, and Co₃O₄ Nanoparticles and Their High Catalytic Performance for Carbon Monoxide and Toluene Oxidation
Yuxi Liu, Hongxing Dai,* Jiguang Deng, Lei Zhang, Zhenxuan Zhao, Xinwei Li, Yuan Wang, Shaohua Xie, Huanggen Yang, and Guangsheng Guo

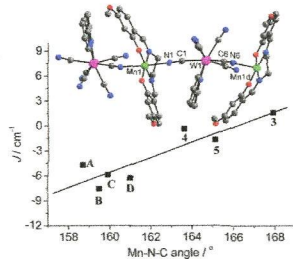
Uniform hollow spherical rhombohedral LaMO₃ and solid spherical cubic MO_x (M = Mn and Co) NPs were fabricated using the PMMA-templating strategy. The higher surface areas and oxygen adspecies concentrations and better low-temperature reducibility are responsible for the excellent catalytic performance of spherical LaCoO₃ and Co₃O₄ NPs for CO and toluene oxidation.



8677  dx.doi.org/10.1021/ic400845z

Cyanide-Bridged W^{VI}Mn^{III} Bimetallic Chains Composed of a Blocked W Hexacyanide Precursor: Geometry-Related Magnetic Couplings and Magnetostructural Correlation
Jin Wuk Lee, Kwang Soo Lim, Dae Won Ryu, Eui Kwan Koh, Sung Won Yoon, Byoung Jin Suh, and Chang Seop Hong*

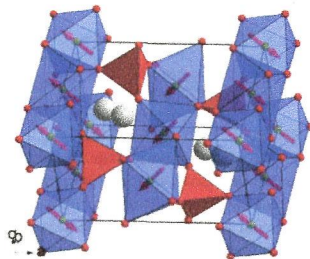
Five one-dimensional W^{VI}Mn^{III} compounds were prepared by self-assembling [W(CN)₆(bpy)]⁻ anions and corresponding Mn Schiff bases. The central geometry around a W atom is taken into consideration to account for the magnetic behavior. In the square antiprismatic systems, a magnetostructural correlation is established in terms of the Mn–N_{ax}–C_{ax} angle in the bridging route.



8685  dx.doi.org/10.1021/ic400870x

Magnetic Structures of NaFePO₄ Maricite and Triphylite Polymorphs for Sodium-Ion Batteries
Maxim Avdeev, Zakhia Mohamed, Chris D. Ling, Jiechen Lu, Mao Tamaru, Atsuo Yamada, and Prabeer Barpanda*

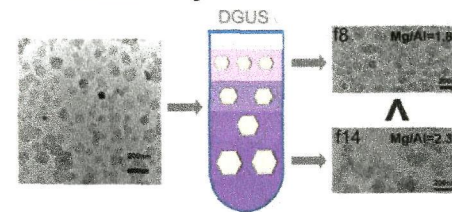
The magnetic structures of olivine NaFePO₄ (triphylite and maricite polymorphs) have been illustrated with the help of magnetic susceptibility, heat capacity, and neutron powder diffraction analyses. Their antiferromagnetic arrangement have been described.




8694  dx.doi.org/10.1021/ic4008763

Synthesis Mechanism Study of Layered Double Hydroxides Based on Nanoseparation
Zheng Chang, Caiying Wu, Sha Song, Yun Kuang, Xiaodong Lei, Liren Wang,* and Xiaoming Sun*

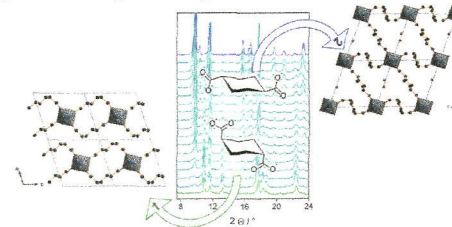
Colloidal layered double hydroxides nanosheets were sorted by their lateral sizes using a density gradient ultracentrifuge separation technique. Composition investigations on these size-sorted nanosheets indicated that larger sheets had higher Mg:Al ratio than the smaller ones. Experiments using different Mg:Al feed ratios confirmed that high Mg:Al ratio induced fast sheet growth speed. Tracking the source of Mg:Al spatial distribution difference in one batch of synthesis at the nucleation process revealed the coprecipitation-redissolution of Mg²⁺.



8699  dx.doi.org/10.1021/ic400825b

Aluminum-1,4-cyclohexanedicarboxylates: High-Throughput and Temperature-Dependent In Situ EDXRD Studies
Felicitas Niekkel, Maximilian Ackermann, Paul Guerrier, André Rothkirch, and Norbert Stock*

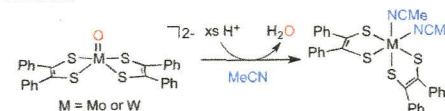
Exploring the use of the flexible aliphatic 1,4-cyclohexanedicarboxylic acid (H₂CDC) as linker molecule in Al-MOF synthesis, two new compounds were discovered. The layered compound **1** is built from chains of corner-sharing AlO₆-polyhedra and *cis*-CDC, while the microporous MIL-53 analogue CAU-13 (**2**) contains the same inorganic building unit as **1** but *trans*-CDC linker molecules in two different conformations. In addition to the detailed characterization of both compounds, the crystallization of **2** was investigated with temperature-dependent in situ EDXRD.



8706  dx.doi.org/10.1021/ic4008747

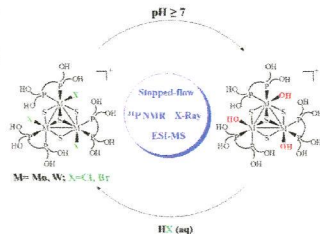
Oxygenation of Mono-oxo Bis(dithiolen) Mo and W Complexes by Protonation
Junhyeok Seo, Paul G. Williard, and Eunsuk Kim*

Protonation-assisted deoxygenation of a mono-oxo molybdenum center has been observed in many oxotransferases when the enzyme removes an oxo group to regenerate a substrate binding site. Such a reaction is reported here with discrete synthetic complexes, [M^{IV}O(S₂C₂Ph₂)₂]²⁻ (M = Mo (**1**), W (**2**)), and the simple protonation in the presence of acetonitrile generates the deoxygenated complexes, [M(MeCN)₂(S₂C₂Ph₂)₂] (M = Mo (**3**), W (**4**)). Differential reactivity between molybdenum and tungsten analogues is also discussed.



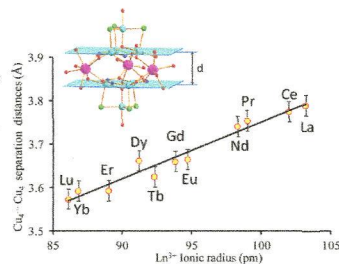
8713 **S** dx.doi.org/10.1021/ic400897y
Influence of the Ligand Alkyl Chain Length on the Solubility, Aqueous Speciation, and Kinetics of Substitution Reactions of Water-Soluble M_3S_4 ($M = Mo, W$) Clusters Bearing Hydroxyalkyl Diphosphines
 Tomás F. Beltrán, Rosa Llusar,* Maxim Sokolov, Manuel G. Basallote,* M. Jesús Fernández-Trujillo, and Jose Ángel Pino-Chamorro

The behavior in aqueous solution of trinuclear Mo and W clusters containing a 1,2-bis(bis(hydroxybutyl)phosphino)ethane ligand coordinated at each metal center differs from that of clusters with the related diphosphine-containing hydroxypropyl substituents, especially in basic solutions where hydroxo complexes are formed instead of complexes resulting from the closure of a chelate ring.



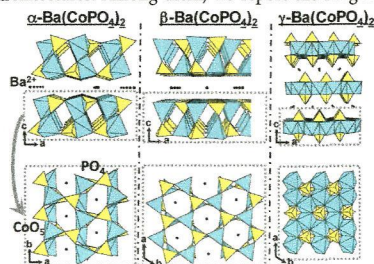
8723 **S** dx.doi.org/10.1021/ic4009015
Lanthanide Triangles Sandwiched by Tetranuclear Copper Complexes Afford a Family of Hendecanuclear Heterometallic Complexes $[Ln^{III}_3Cu^{II}_8]$ ($Ln = La-Lu$): Synthesis and Magnetostructural Studies
 Olga Iasco, Ghenadie Novitchi,* Erwann Jeanneau, and Dominique Luneau*

A family of hendecanuclear heterometallic clusters $[Ln^{III}_3Cu^{II}_8]$ ($Ln = La-Lu$) are reported. The central core of isomorphous clusters is made of a triangle of lanthanide ions sandwiched between two tetranuclear copper(II) clusters. The separation distance between the two $\{Cu_4\}$ clusters in $[Ln^{III}_3Cu^{II}_8]$ varies linearly with the ionic radius of the lanthanide ions. The studies of the magnetic properties of the series show that only the dysprosium compound displays single-molecule magnet behavior.



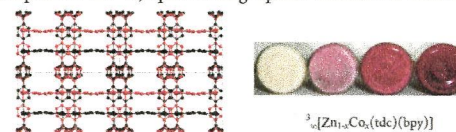
8732 **S** dx.doi.org/10.1021/ic4009027
Puzzling Polymorphism of Layered $Ba(CoPO_4)_2$
 Rénaud David, Houria Kabbour, Alain Pautrat, and Olivier Mentré*

The thermal study of the layered Co^{2+} -based compounds $Ba(CoPO_4)_2$ shows a peculiar phase diagram with the apparition of several forms dominated by layered architectures. Among them, we report the long-awaited structure of α - $Ba(CoPO_4)_2$



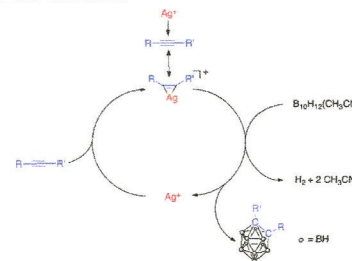
8738 **S** dx.doi.org/10.1021/ic400857s
Synthesis, Crystal Structure and Catalytic Behavior of Homo- and Heteronuclear Coordination Polymers $[M(tdc)(bpy)]$ ($M^{2+} = Fe^{2+}, Co^{2+}, Zn^{2+}, Cd^{2+}$; $tdc^{2-} = 2,5$ -thiophenedicarboxylate)
 Florian Kettner, Christian Worch, Jens Moellmer, Roger Gläser, Reiner Staudt, and Harald Krautscheid*

On the basis of the isostructural crystallization of a series of 3D coordination polymers, the related heteronuclear compounds are accessible by isomorphous substitution. Introduction of Co^{2+} ions into the framework of $[Zn(tdc)(bpy)]$ generates activity in the catalytic oxidation of alkenes, as shown for the test reaction of cyclooctene with *tert*-butyl hydroperoxide. The title compounds are thermally stable up to ca. 400 °C, upon heating a phase transition is initiated by the loss of solvent molecules.



8743 **S** dx.doi.org/10.1021/ic400928v
High Yielding Preparation of Dicarba-*closo*-dodecaboranes Using a Silver(I) Mediated Dehydrogenative Alkyne-Insertion Reaction
 Antonio Toppino, Afaf R. Genady, Mohamed E. El-Zaria, James Reeve, Fargol Mostofian, Jeff Kent, and John F. Valliant*

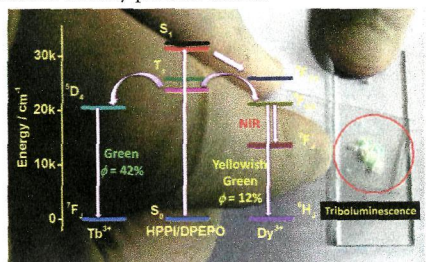
A series of coinage metal salts were screened to identify compounds that would enhance the yields of *ortho*-caboranes produced using alkynes and $B_{10}H_{12}(CH_3CN)_2$. $AgNO_3$ in catalytic amounts increased yields significantly for a variety of mono- and polyfunctional internal and terminal alkynes. $AgNO_3$ appears to prevent unwanted reduction/hydroboration of the alkyne starting material prior to carborane formation.



Brilliant Photoluminescence and Triboluminescence from Ternary Complexes of Dy^{III} and Tb^{III} with 3-Phenyl-4-propanoyl-5-isoxazonate and a Bidentate Phosphine Oxide Coligand

S. Biju, N. Gopakumar, J.-C. G. Bünzli,* R. Scopelliti, H. K. Kim,* and M. L. P. Reddy*

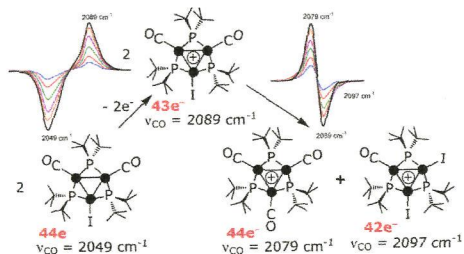
Thermally stable and highly luminescent complexes of Dy^{III} and Tb^{III} have been synthesized by careful selection of a heterocyclic β -diketone and a phosphine oxide coligand. The lifetime and overall quantum yield obtained for the Dy^{III} complexes are the largest values reported so far for Dy^{III}-tris- β -diketonates; this complex also exhibits substantial NIR luminescence. Most importantly, the crystals of both Tb^{III} and Dy^{III} complexes show efficient triboluminescence. Hence, these molecules may find potential applications in many photonic devices.



Synthesis and Spectroscopic and Spectroelectrochemical Characterization of a New Family of 44e⁻ Tris-Phosphido-Bridged Palladium Triangles

Veronica Bonuccelli, Tiziana Funaioli, Piero Leoni,* Fabio Marchetti, and Lorella Marchetti

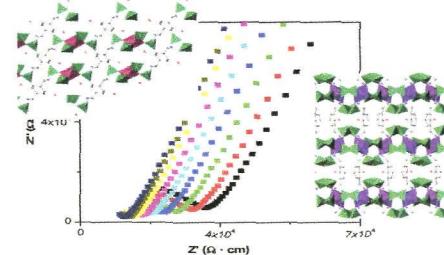
Triangular clusters containing a $[M_3(\mu\text{-PR}_2)_3]^+$ core are very common in platinum chemistry but were virtually unknown for $M = \text{Pd}$. Herein we describe the synthesis and characterization of several palladium derivatives belonging to this class. They exhibit at least one reversible monoelectronic oxidation yielding relatively stable 43e⁻ cations, one of which, $[\text{Pd}_3(\mu\text{-PBu}_2)_3(\text{CNBu}_t)_3](\text{PF}_6)_2$, was also isolated as a thermally stable solid by chemical oxidation with AgPF_6 of the parent 44e⁻ species.



Structural Variability in Multifunctional Metal Xylenediaminetetraphosphonate Hybrids

Rosario M. P. Colodrero, Giasemi K. Angeli, Montse Bazaga-Garcia, Pascual Olivera-Pastor, Didier Villemin, Enrique R. Losilla, Estefania Q. Martos, Gary B. Hix, Miguel A. G. Aranda, Konstantinos D. Demadis,* and Aurelio Cabeza*

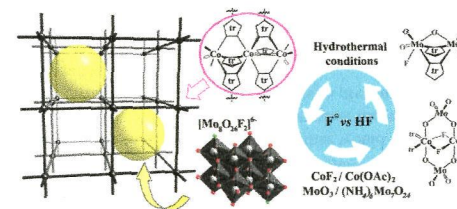
Two new families of divalent metal hybrid derivatives from the aromatic tetraphosphonic acids 1,4- and 1,3-bis(aminomethyl)benzene-*N,N'*-bis(methylenephosphonic acid), $(\text{H}_2\text{O}_3\text{PCH}_2)_2\text{-N-CH}_2\text{C}_6\text{H}_4\text{CH}_2\text{-N}(\text{CH}_2\text{PO}_3\text{H}_2)_2$ [$M-(p\text{-H}_6\text{L})$ and $M-(m\text{-H}_6\text{L})$], have been synthesized under mild conditions. Isostructural $M-(p\text{-H}_6\text{L})$ compounds show monodimensional frameworks, while $M-(m\text{-H}_6\text{L})$ compounds exhibit a 3D pillared open-framework with small channels filled with water molecules. The behavior of these compounds as multifunctional materials for photoluminescence, in corrosion protection, and/or as proton conductor solids has been evaluated.



Unprecedented Trapping of Difluoroctamolybdate Anions within an α -Polonium Type Coordination Network

Olena V. Sharga, Andrey B. Lysenko,* Marcel Handke, Harald Krautscheid, Eduard B. Rusanov, Alexander N. Chernega, Karl W. Krämer, Shi-Xia Liu,* Silvio Decurtins, Adam Bridgeman, and Konstantin V. Domasevitch

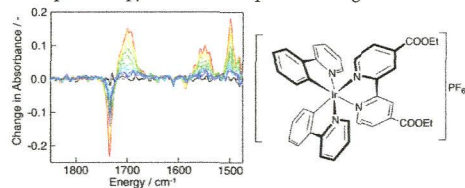
1,2,4-Triazolyl ligands can be employed in the construction of $\text{Co}^{\text{II}}/\text{Mo}^{\text{VI}}$ fluorinated hybrid solids. A unique example of incorporation of difluoroctamolybdate anions $[\text{Mo}_8\text{O}_{26}\text{F}_2]^{6-}$ into the α -Po-type coordination network based on the $[\text{Co}_3(\mu\text{-tr})_6]^{6+}$ SBU has been demonstrated. The presence of HF/F^- in the reaction systems seems to be the most likely factor predetermining the Mo^{VI} oxo fluoride condensation or formation of the $\text{F}^-/\text{MoO}_4^{2-}$ mixed-anion species.



Tracking of Tuning Effects in Bis-Cyclometalated Iridium Complexes: A Combined Time Resolved Infrared Spectroscopy, Electrochemical, and Computational Study

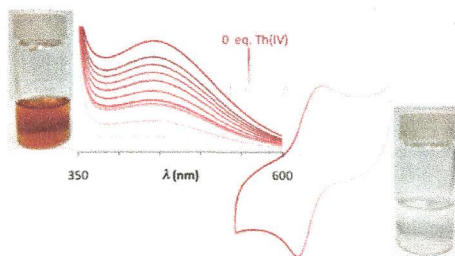
Danielle N. Chirdon, Catherine E. McCusker, Felix N. Castellano,* and Stefan Bernhard*

Time resolved infrared spectroscopy (TRIR) was used to study the long-lived excited state in a series of increasingly fluorinated iridium complexes. TRIR spectra show that the first excitation has mixed MLCT/ligand-to-ligand transfer character throughout the series. Photoluminescence, transient absorption spectroscopy, and DFT calculations support the TRIR findings while electrochemistry shows expected tuning of the HOMO and LUMO. Transitions beyond the lowest-lying excited state are viewed via UV-vis spectroscopy which is interpreted through TD-DFT.

**Solution Thermodynamic Stability of Complexes Formed with the Octadentate Hydroxypyridinonate Ligand 3,4,3-Li(1,2-HOPO): A Critical Feature for Efficient Chelation of Lanthanide(IV) and Actinide(IV) Ions**

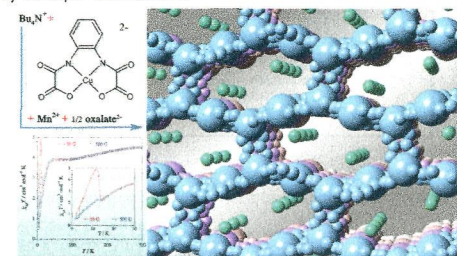
Gauthier J.-P. Deblonde, Manuel Sturzbecher-Hoehne, and Rebecca J. Abergel*

The solution thermodynamics of water soluble complexes formed between Ce(III), Ce(IV), Th(IV) and the octadentate chelating agent 3,4,3-Li(1,2-HOPO) were investigated. Several techniques including spectrofluorimetric and automated spectrophotometric titrations were used to take advantage of the unique spectral properties of the hydroxypyridinonate chelator and overcome the slow spontaneous oxidation of associated Ce(III) complexes ($\log \beta_{110} = 17.4(5)$) and the extraordinarily high stability of the corresponding Ce(IV) and Th(IV) complexes ($\log \beta_{110} = 41.5(5)$ and $40.1(5)$, respectively).

**A Two-Dimensional Oxamate- and Oxalate-Bridged Cu^{II}Mn^{II} Motif: Crystal Structure and Magnetic Properties of (Bu₄N)₂[Mn₂{Cu(opba)}₂ox]**

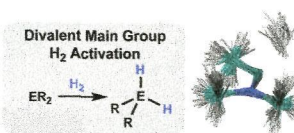
Maria V. Marinho, Tatiana R. G. Simões, Marcos A. Ribeiro, Cynthia L. M. Pereira, Flávia C. Machado, Carlos B. Pinheiro, Humberto O. Stumpf, Joan Cano,* Francesc Lloret, and Miguel Julve

(Bu₄N)₂[Mn₂{Cu(opba)}₂ox]: a new spin-canted molecule-based magnet built by the stacking of anionic honeycomb-like networks partially penetrated by n-Bu₄N⁺ counterions.

**Theory of Divalent Main Group H₂ Activation: Electronics and Quasiclassical Trajectories**

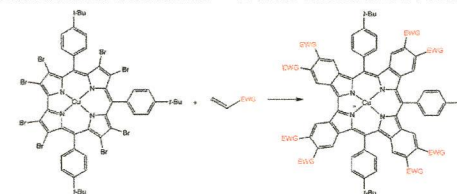
Deepa Devarajan, Charles E. Doubleday,* and Daniel H. Ess*

Energy decomposition analysis and quasiclassical trajectories were combined to provide a comprehensive picture of H₂ addition to carbon, Si, and Ge singlet divalent main group compounds.

**Synthesis and Characterization of Functionalized meso-Triaryltetrabenzocorroles**

Giuseppe Pomarico, Sara Nardis, Manuela Stefanelli, Daniel O. Cicero, M. Graça H. Vicente, Yuanyuan Fang, Ping Chen, Karl M. Kadish,* and Roberto Paolesse*

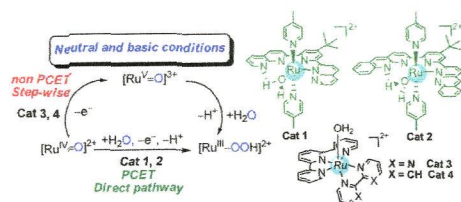
5,10,15-Triaryltetrabenzocorroles are prepared via a Heck reaction when an electron-withdrawing group is present on the reacting olefin. The influence of these substituents on the corrole properties is studied in detail by spectroscopic, electrochemical, and spectroelectrochemical characterization of these functionalized corroles.



8845 **5** dx.doi.org/10.1021/ic401023w
Water Oxidation with Mononuclear Ruthenium(II) Polypyridine Complexes Involving a Direct $Ru^{IV}=O$ Pathway in Neutral and Alkaline Media

Yosra M. Badiei, Dmitry E. Polyansky,* James T. Muckerman, David J. Szalda, Rubabe Haberdar, Ruifa Zong, Randolph P. Thummel, and Etsuko Fujita*

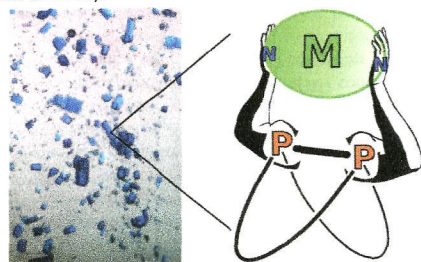
The pH-dependent onset catalytic potentials indicate that Cat 1 and Cat 2 follow the thermodynamically more favorable "direct pathway" via $[Ru^{IV}=O]^{2+}$, in neutral and basic media. However, in the cases of $[Ru(tpy)(bpy)(OH_2)]^{2+}$ and $[Ru(tpy)(bpm)(OH_2)]^{2+}$, the formation of the $Ru^{IV}=O$ species appears to be required before O–O bond formation. Cat 1 and Cat 2 provide a unique functional model for water oxidation that proceeds by four consecutive PCET steps in neutral and alkaline media.



8851 **5** dx.doi.org/10.1021/ic401052a

Functionalization Reactions Characteristic of a Robust Bicyclic Diphosphane Framework
 Daniel Tofan, Manuel Temprado,* Subhōjit Majumdar, Carl D. Hoff,* and Christopher C. Cummins*

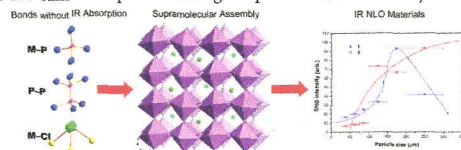
The bicyclic diphosphane $P_2(C_6H_{10})_2$ framework displayed an unprecedented selectivity toward mono- or bis-functionalization without cleavage of the P–P bond. The formation of chalcogenide phosphines was investigated in detail via computational and calorimetric methods. The symmetric diiminodiphosphorane $(MesN)_2P_2(C_6H_{10})_2$ was studied as a preorganized ligand for coordination chemistry.



8865 **5** dx.doi.org/10.1021/ic401056t
Large Mid-IR Second-Order Nonlinear-Optical Effects Designed by the Supramolecular Assembly of Different Bond Types without IR Absorption

Xiao-Ming Jiang, Guan-E Wang, Zhi-Fa Liu, Ming-Jian Zhang, and Guo-Cong Guo*

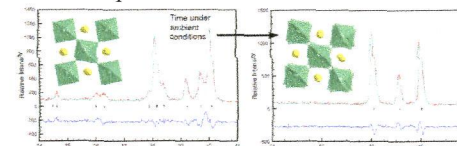
Two new different-bond-type hybrid compounds, $(Hg_6P_4Cl_3)(PbCl_3)$ (1) and $(Hg_{23}P_{12})(ZnCl_4)_6$ (2), with supramolecular interactions in the structures, show large second-harmonic-generation activity and are transparent in the wide mid-IR region, providing an effective route for searching new IR nonlinear-optical material systems by combining two or more different bond types with no IR absorption in the same compound through supramolecular assembly.



8872 **5** dx.doi.org/10.1021/ic401061t

Unusual Phase Behavior in the Piezoelectric Perovskite System, $Li_xNa_{1-x}NbO_3$
 Martin D. Peel, Sharon E. Ashbrook, and Philip Lightfoot*

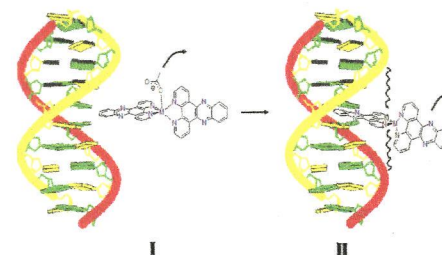
The phases present in the solid solution $Li_xNa_{1-x}NbO_3$ have been studied using a combination of diffraction and NMR methods. For the region $0.08 < x < 0.20$ a subtle phase competition is observed, which includes transformation of one phase to another for samples standing at ambient temperature.



8881 **5** dx.doi.org/10.1021/ic401067d

Nonclassical Metallointercalators with Dipyridophenazine: DNA Interaction Studies and Leishmanicidal Activity
 João Madureira,* Catarina I. V. Ramos, Mónica Marques, Carla Maia, Bruno de Sousa, Lenea Campino, M. Graça Santana-Marques, and Nicholas Farrell*

$[Cu(II)(dppz)_2(AcOO)]^+$ and $[Zn(II)(dppz)_2]^{2+}$ bind DNA by intercalation and covalent binding modes. A loss of a dppz unit, which occurs only when DNA is present, justifies such dual binding mode. The proposed interaction mechanism results from combined biophysical data from thermal denaturation, CD, rheometry, AFM and QTof-ESI-MS. DNA saturation occurs for copper at about half the concentration of zinc, apparently due to the increased ability of $Cu(II)$ to distort to a more planar structure.

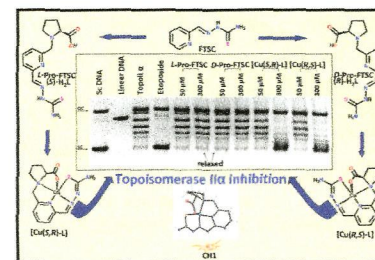


8895 **5** dx.doi.org/10.1021/ic401079w

Copper(II) Complexes with Highly Water-Soluble l- and d-Proline–Thiosemicarbazone Conjugates as Potential Inhibitors of Topoisomerase II α

Felix Bacher, Éva A. Enyedy,* Nóra V. Nagy, Antal Rockenbauer, Gabriella M. Bognár, Robert Trondl, Maria S. Novak, Érik Klapproth, Tamás Kiss, and Vladimír B. Arion*

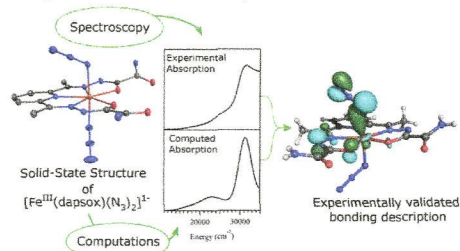
Copper(II) complexes with highly water-soluble thiosemicarbazone–proline conjugates, namely, $[Cu(S,R)-L]$ and $[Cu(R,S)-L]$, exhibit Topoisomerase II α inhibitory potential in a DNA plasmid relaxation assay and antiproliferative activity in CH1 ovarian carcinoma cells.



8909  dx.doi.org/10.1021/ic401098x

Structural, Spectroscopic, and Computational Characterization of the Azide Adduct of Fe^{III}(2,6-diacetylpyridinebis(semioxamamide)), a Functional Analogue of Iron Superoxide Dismutase
Craig T. Gutman, Ilia A. Guzei, and Thomas C. Brunold*

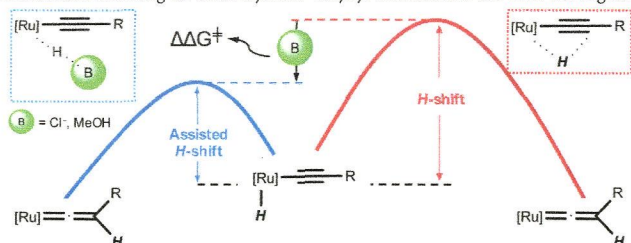
We have prepared and characterized [Fe^{III}(dapsox)(N₃)₂]⁻ (**1**), where dapsox = 2,6-diacetylpyridinebis(semioxamamide), which models an intermediate that is formed in the reaction of Fe(dapsox), a functional mimic of Fe superoxide dismutase (FeSOD), with O₂⁻. Collectively, our X-ray crystallographic, spectroscopic, and computational studies of **1** reveal that the Fe–N₃ bonding interactions are similar to those in the azide adduct of FeSOD, consistent with the rapid reaction of **1** with superoxide and supporting an inner-sphere mechanism of catalysis.



8919  dx.doi.org/10.1021/ic401119p

Counteranion and Solvent Assistance in Ruthenium-Mediated Alkyne to Vinylidene Isomerizations
Manuel Jiménez-Tenorio,* M. Carmen Puerta,* Pedro Valerga, Manuel A. Ortuño, Gregori Ujaque, and Agustí Lledós*

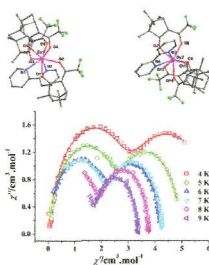
The presence of Cl⁻ or MeOH in solutions with metastable π -alkyne complexes [Cp*₂Ru(η^2 -HC≡CR)(ⁱPr₂PNHPy)][BPh₄] (R = COOMe, C₆H₄CF₃) causes an acceleration in the rate of isomerization to the corresponding vinylidene complexes [Cp*₂Ru=C=CHR)(ⁱPr₂PNHPy)][BPh₄] (R = COOMe, C₆H₄CF₃). According to DFT calculations, a base-assisted hydrogen migration mechanism involving an acidic hydrido-alkynyl intermediate has been envisaged.



8933  dx.doi.org/10.1021/ic4011218

Field-Induced Single-Ion Magnets Based on Enantiopure Chiral β -Diketonate Ligands
Cai-Ming Liu,* De-Qing Zhang, and Dao-Ben Zhu

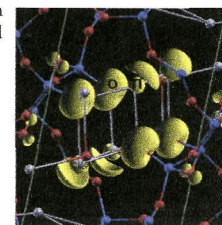
Two homochiral Dy(III) β -diketonate stereoisomers with the 2,2'-bipyridine capping ligand are cocrystallized together, displaying field-induced single-ion magnet behaviors with two separate relaxation processes; as a reference, no stereoisomerization happens for the homochiral Dy(III) β -diketonate with the 1,10-phenanthroline coligand, exhibiting a single relaxation process of the magnetization.



8941  dx.doi.org/10.1021/ic401118s

Structural, Spectroscopic, and Computational Studies on Ti₄Si₂O₁₂: A Microporous Thallium Silicate
Volker Kahlenberg,* Lukas Perfler, Jürgen Konzett, and Peter Blaha

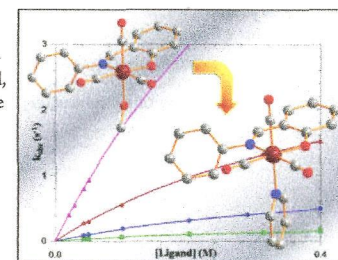
Single crystals of the previously unknown thallium silicate Ti₄Si₂O₁₂ have been prepared from hydrothermal crystallization of a glassy starting material at 500 °C and 1kbar. The compound can be classified as an interrupted framework silicate with Q³- and Q⁴-units in the ratio 2:1. Within the framework 4-, 6-, and 12-membered rings can be distinguished.



8950  dx.doi.org/10.1021/ic401115j

Activation of Rhenium(I) Toward Substitution in *fac*-[Re(*N,O'*-Bid)(CO)₃(HOCH₃)] by Schiff-Base Bidentate Ligands (*N,O'*-Bid)
Alice Brink, Hendrik G. Visser, and Andreas Roodt*

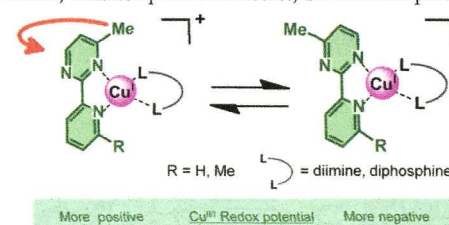
Activation of rhenium(I) in different *fac*-[Re(*N,O'*-Bid)(CO)₃(H₂O)] complexes (*N,O'*-Bid = monoanionic bidentate Schiff-base ligands), as manifested by the methanol substitution from a preselected range of pyridine-type monodentate entering ligands, are reported. Saturation kinetics is observed, and together with the activation entropy, provide supporting evidence that the process proceeds via a dissociative interchange mechanism.




8962  dx.doi.org/10.1021/ic4011295

Structural Modification on Copper(I)-pyridylpyrimidine Complexes for Modulation of Rotational Dynamics, Redox Properties, and Phototriggered Isomerization

Michihiro Nishikawa, Yusuke Takara, Yohei Hattori, Kuniharu Nomoto, Tetsuro Kusamoto, Shoko Kume,* and Hiroshi Nishihara*
A newly synthesized compound, [Cu(Mepypp)(L_{Mes})]BF₄ (1-BF₄, where Mepypp = 4-methyl-2-(2'-pyridyl)pyrimidine and L_{Mes} = 2,9-dimesityl-1,10-phenanthroline), was compared with similar complexes that have been previously reported complexes. The presence and location of methyl substituents on the pyridine moiety increased steric repulsion and contributed to quicker ligand rotation, enhanced photoluminescence, and increased photodriven rotational isomerization.

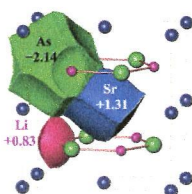


8971  dx.doi.org/10.1021/ic401166v

Synthesis, Structure, and Properties of Two Zintl Phases around the Composition SrLiAs

Xian-Juan Feng, Yurii Prots, Marcus Peter Schmidt, Stefan Hoffmann, Igor Veremchuk, Walter Schnelle, Ulrich Burkhardt, Jing-Tai Zhao, and Yuri Grin*

Two atomic arrangements were found near the equiatomic composition in the strontium–lithium–arsenic system: *o*-SrLiAs with TiNiSi structure type, space group *Pnma*; *h*-SrLi_{1-x}As with ZrBeSi structure type, space group *P6₃/mmc*. Electron density analysis within the framework of the quantum theory of atoms in molecules revealed the charge transfer according to Sr^{1.3+}Li^{0.8+}As^{2.1-}, agreeing with the electronegativity of the elements. Magnetic susceptibility measurements indicate a diamagnetic character of both phases, which verifies calculated electronic density of states.

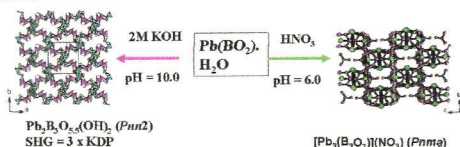


8979  dx.doi.org/10.1021/ic401175r

Pb₂B₃O_{5.5}(OH)₂ and [Pb₃(B₃O₇)](NO₃): Facile Syntheses of New Lead(II) Borates by Simply Changing the pH Values of the Reaction Systems

Jun-Ling Song, Chun-Li Hu, Xiang Xu, Fang Kong, and Jiang-Gao Mao*

Using lead(II) metaborate as starting material, by only adjusting pH values of the reaction system, four lead(II) borates were obtained in high yields by hydrothermal reactions, two of which are new. The polar Pb₂B₃O_{5.5}(OH)₂ features a novel 3D anionic network with large 14 member ring tunnels composed of unique 1D boron-oxide chains and dimeric B₂O₇ groups, which are filled by the Pb²⁺ cations.

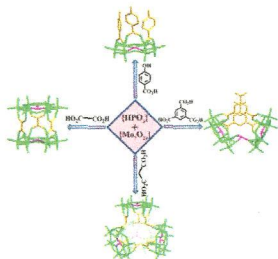


8987  dx.doi.org/10.1021/ic401176j

Carboxylate-Functionalized Phosphomolybdates: Ligand-Directed Conformations

Donghui Yang, Suzhi Li, Pengtao Ma, Jingping Wang,* and Jingyang Niu*

The [HPMo₆O₂₁]²⁻ units and carboxylate linkers can be combined to build novel polyanions by a carefully designed complementary system in self-assembly processes depending only on the number of carboxyl groups and the nature of carboxylic acids.

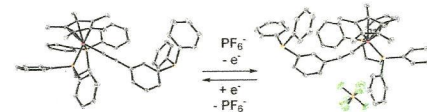


8993  dx.doi.org/10.1021/ic4011828

Triarylphosphine Ligands with Pendant Electron-Rich “[Fe(κ²-dppe)(η⁵-C₅Me₅)(C≡C)]⁻” Substituents

Ayham Tohmé, Guillaume Grelaud, Gilles Argouarch, Thierry Roisnel, Arnaud Bondon, and Frédéric Paul*

Four new triarylphosphines ligands featuring peripheral electron-rich and redox-active organometallic “[Fe(κ²-dppe)(η⁵-C₅Me₅)(C≡C)]⁻” pendant substituents are reported. The steric and electronic properties of these metallo-phosphines, which are stable and isolable under two redox-states, are discussed.

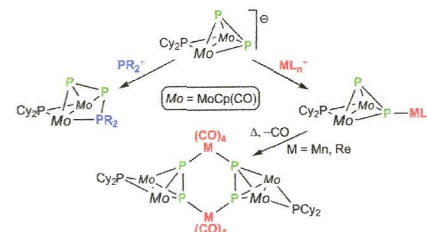


9005  dx.doi.org/10.1021/ic401204j

Reactivity of the Anionic Diphosphorus Complex [Mo₂Cp₂(μ-PCy₂)(μ-κ²-x²-P₂)(CO)₂]⁻ toward Phosphorus- and Transition Metal-Based Electrophiles

M. Angeles Alvarez, M. Esther García, Daniel García-Vivó, Raquel Lozano, Alberto Ramos,* and Miguel A. Ruiz*

The title anion reacts with chlorophosphines to give unprecedented phosphinodiphosphenyl (P₂PR₂) complexes resulting from the insertion of the carbene-like PR₂⁺ cations in one of the Mo–P bonds of the anion, while its reaction with different transition-metal halide complexes [MXL_n] (with L being a Cp or CO ligand) lead in all cases to the “end-on” binding of the organometallic fragment ML_n to the basal P atom of the anion.

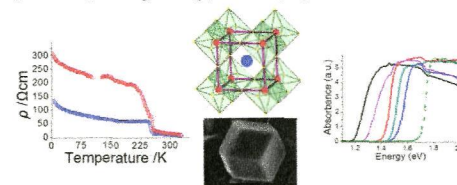


9019  dx.doi.org/10.1021/ic401215x

Semiconducting Tin and Lead Iodide Perovskites with Organic Cations: Phase Transitions, High Mobilities, and Near-Infrared Photoluminescent Properties

Constantinos C. Stoumpos, Christos D. Malliakas, and Mercouri G. Kanatzidis*

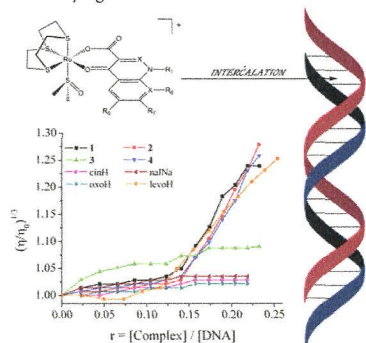
The hybrid iodide perovskites of Sn and Pb have been long considered as puzzling compounds displaying a metal-like conductivity. The results demonstrated here provide solid evidence for the semiconducting nature of this family of compounds that display high carrier mobilities and ambient temperature photoluminescence. Moreover, the compounds show tunable charge-transport and optical properties depending strongly on the preparation method.



New Uses for Old Drugs: Attempts to Convert Quinolone Antibacterials into Potential Anticancer Agents Containing Ruthenium

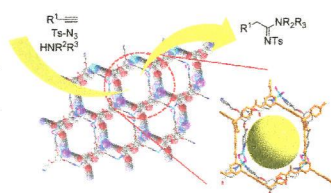
Jakob Kljun, Ioannis Bratsos, Enzo Alessio, George Psomas, Urška Repnik, Miha Butinar, Boris Turk, and Iztok Turel*

Four novel ruthenium-quinolone complexes bearing the face-capping ligand trithiacyclononane were synthesized. The complexes, which quickly bind serum albumins and are capable of intercalating CT DNA, exhibit moderate activity against cathepsins B and S, and show a modest activity against one of the tested cancer cell lines.

**Porous Metal–Organic Framework Catalyzing the Three-Component Coupling of Sulfonyl Azide, Alkyne, and Amine**

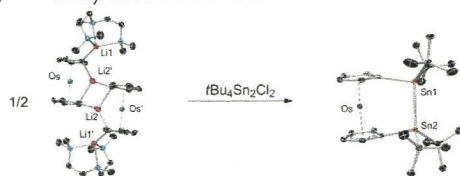
Tao Yang, Hao Cui, Changhe Zhang, Li Zhang,* and Cheng-Yong Su*

The robustly porous metal–organic framework, MOF–Cu₂I₂(BTTP4), can efficiently catalyze the three-component coupling of sulfonyl azide, alkyne, and amine, leading to the formation of important organic compounds of amidines in high yields.

**Structure and Reactivity of Distanna[2]metallocenophanes of Ruthenium and Osmium**

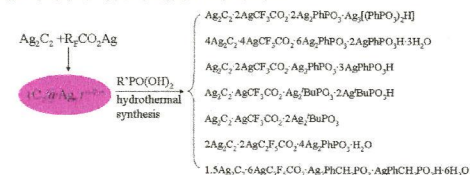
Holger Braunschweig,* Florian Hupp, Thomas Kramer, and Julian Mager

We report the molecular structures of 1,1'-dilithiometallocenes of ruthenium and osmium. These compounds served as precursors for the synthesis and subsequent structural characterization of the first [2]osmocenophanes with disilane and distanna bridges, as well as of a distanna[2]ruthenocenophane. In addition, the insertion of sulfur and selenium into the Sn–Sn bridges was studied and it was observed that the presence of the Lewis base pmdta (*N,N,N',N'',N'''*-pentamethyldiethylenetriamine) dramatically accelerates the reaction.

**Silver(I) Multiple Salts Assembled with Phosphonate, Perfluorocarboxylate, and the Multinuclear Silver–Ethyne Diide Supramolecular Synthons**

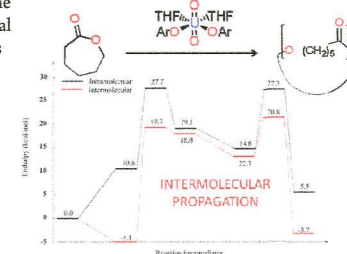
Ting Hu and Thomas C. W. Mak*

Combining phosphonate and perfluorocarboxylate ligands with silver ethynediide, a series of seven new multiple salts have been synthesized under hydrothermal conditions and characterized by X-ray crystallography. The phosphonate ligands employed include phenylphosphonate, *tert*-butylphosphonate, and benzylphosphonate, and different complexes can be obtained by variation of the mole ratios of the reactants. The C₂²⁻ species in all compounds is invariably located inside a polyhedral or partially opened silver(I) cage of six to nine vertices. Six compounds exhibit coordination layer structures, while the remaining one has a three-dimensional coordination framework.

**New Mechanism for the Ring-Opening Polymerization of Lactones? Uranyl Aryloxide-Induced Intermolecular Catalysis**

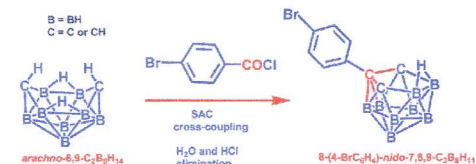
Aurora Walshe, Jian Fang, Laurent Maron,* and Robert J. Baker*

Uranyl aryloxide compounds act as ring-opening polymerization catalysts for the lactones δ -valerolactone and ϵ -caprolactone. A spectroscopic and computational study shows that the mechanism is intermolecular, which is the first time this pathway has been invoked for lactone polymerization.

**Carbon Insertion into *arachno*-6,9-C₂B₈H₁₄ via Acyl Chlorides. Skeletal Alkylcarbonation (SAC) Reactions: A New Route for Tricarbollides**

Mario Bakardjiev, Bohumil Štibr,* Josef Holub, Zdeňka Padělková, and Aleš Růžička

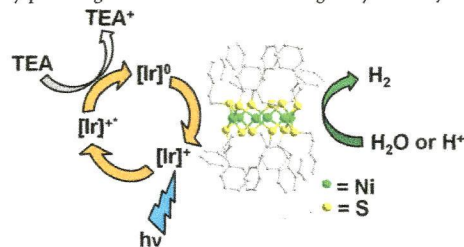
Reactions between *arachno*-6,9-C₂B₈H₁₄ and acyl chlorides (RCOCl) generate a series of alkylated and arylated tricarbollides 8-*R-nido*-7,8,9-C₂B₈H₁₁ in high yields. These skeletal alkylcarbonation (SAC) reactions are reminiscent of aldol condensation and are consistent with a unique insertion of the carbonyl carbon into the structure of 6,9-C₂B₈H₁₄ under elimination of the three carborane extra hydrogen atoms as H₂O and HCl, and result in effective cross-coupling between R and the tricarbaborane cage.



Photocatalytic Hydrogen Generation System Using a Nickel-Thiolate Hexameric Cluster

Husain N. Kagalwala, Eric Gottlieb, Gao Li, Tao Li, Rongchao Jin, and Stefan Bernhard*

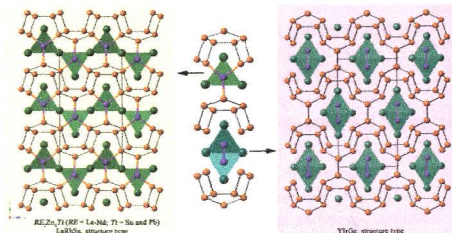
Photocatalytic hydrogen generation from water was achieved using a nickel hexameric cluster, $Ni_6(SCH_2CH_2Ph)_6$, $Ph = C_6H_5$, and an iridium-based photosensitizer, $[Ir(F\text{-}mppy)_2(dtbbpy)](PF_6)$. The Ni_6 cluster demonstrated the ability to evolve hydrogen electrocatalytically (HER), justifying its use as a water reducing catalyst (WRC). High catalytic turnover numbers (TONs) and frequencies (TOFs) were obtained at optimal Ir and Ni_6 concentrations. Dynamic quenching studies shed light on the mechanism while mercury poisoning tests determined the homogeneity of the system.



New Polar Intermetallic Phases RE_2Zn_3Tt ($RE = La-Nd$; $Tt = Sn$ and Pb): Synthesis, Structure, Chemical Bonding, and Magnetic Properties

Nian-Tzu Suen and Svilen Bobev*

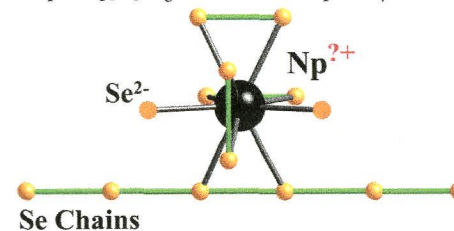
The focus of this paper is on the crystal and electronic structures of the new polar intermetallic phases RE_2Zn_3Tt ($RE = La-Nd$; $Tt = Sn$ and Pb). A prominent structural feature is the trigonal-planar coordination of the Tt atoms.



Reinvestigation of Np_2Se_5 : A Clear Divergence from Th_2S_5 and Th_2Se_5 in Chalcogen–Chalcogen and Metal–Chalcogen Interactions

Geng Bang Jin,* Yung-Jin Hu, Brian Bellott, S. Skanthakumar, Richard G. Haire, L. Soderholm, and James A. Ibers

The main difference among related structures of Np_2Se_5 , Th_2Se_5 , and Th_2S_5 lies in the chalcogenide sublattice. The implications of this difference are examined in terms of different chalcogen–chalcogen and metal–chalcogen interactions, and ionic radii. XANES and magnetic susceptibility data of Np_2Se_5 complement the structural findings. Our results provide evidence that the valence state of Np in Np_2Se_5 is greater than +3 and probably less than +4.



Iridium and Ruthenium Catalyzed Syntheses, Hydroborations, and Metathesis Reactions of Alkenyl-Decaboranes

Shahana Chatterjee, Patrick J. Carroll, and Larry G. Sneddon*

The selective syntheses of both the β -E- and the α -olefin isomers of the previously unknown 6-alkenyl-, 6,9-dialkenyl-, and 6-alkyl-9-alkenyl-decaboranes in which the olefin group is directly bonded to a cage-boron have been achieved via iridium and ruthenium catalyzed decaborane and 6-alkyl-decaborane alkyne-hydroborations. These alkenyl-decaboranes can then be readily converted to other useful derivatives, including coupled-cage and functionally substituted compounds, via iridium-catalyzed hydroborations and ruthenium-catalyzed homo and cross olefin-metathesis reactions.

